SKI Report 99:25

Ultrasonic Characterization of Defects

Part 4. Study of Realistic Flaws in Welded Carbon Steel

Fredrik Lingvall
Tadeusz Stepinski

February 1999

ISSN 1104-1374
ISRN SKI-R--99/25--SE

SKI

SKI Report 99:25

Ultrasonic Characterization of Defects

Part 4. Study of Realistic Flaws in Welded Carbon Steel

Fredrik Lingvall
Tadeusz Stepinski

Uppsala University, Signals and Systems
Box 528, SE-751 20 Uppsala, Sweden

February 1999

SKI Project Number 97040

Abstract

This report treats the ultrasonic measurements performed on the new V-welded carbon steel blocks and development of the algorithms for feature extraction, flaw position estimation, etc. Totally 36 different defects, divided into 8 types, were manufactured and implanted into the V-welds in the steel blocks. The flaw population can also be divided in two major groups: sharp flaws (various types of cracks and lack of fusion) and soft types of flaws (slag, porosity and over penetration). A large amount of B- and D-scan measurements were performed on these flaws using 6 different transducers. The evaluation of these measurements resulted in the conclusion that the signal variation for the same type of defects is rather large compared to the variation found in signals from artificial and simulated defects. The steel block measurements also revealed that some of the defects were hard to distinguish, particularly if traditional features like fall/raise times, pulse duration and echo dynamics are used. To overcome this difficulty more powerful feature extraction methods were proposed, like the discrete wavelet transform and principal component analysis. Another important subject that is treated in this report is the estimation of flaw positions from B-scans. The previously used, one dimensional method, appeared to be sensitive to errors in the steel block measurements which, in some cases, resulted in poor flaw position estimates. Therefore, a two dimensional approach was proposed which should result in more robust estimates due to the larger amount of data that is used for the estimation.

Sammanfattning

Denna rapport innehåller resultat från de mätningar som har gjorts på de nytillverkade stålblocken innehållande en V-svets med inplanterade "naturliga" defekter. Rapporten beskriver också de algoritmer som använts för estimering av position hos defekter, särdrags extraktion (eng. feature extraction) mm. Totalt fanns det 36 olika defekter i stålblocken indelat i 8 olika typer. Defekterna kan också delas in i två huvudgrupper: skarpa defekter (sprickor etc) och mjuka (inklusioner, prorositet etc). Ett större antal B- och D-scan har samlats in med 6 olika sökare från dessa defekter. Utvärderingar av dessa mätningar visar att variationen hos signalen inom en defekttyp är stor jämfört med motsvarande mätningar gjorda för simulerade och artificiella defekter. Det har även visat sig att det är svårt att skilja på vissa typer av defekter vilket betyder att vi förmodligen har överlappande beslutsområden. Detta är speciellt tydligt om vi använder klassiska metoder för särdrags-extraktion som stigtid, falltid, pulslängd och ekodynamik. På grund av detta föreslås användning av mera kraftfulla metoder för att extrahera särdrag vilka behåller mera information om ultraljudssignalen än vad de klassiska metoderna gör. Två förslag till sådana metoder är den diskreta wavelet transformen och PCA (principal component analysis). Vidare behandlas också estimering av position hos defekter vilken är vital eftersom positionen hos en defekt används för den senare djupnormeringen av ultradjudssiganlen. Det har visat sig att den tidigare använda (en dimensionella) metoden för att hitta defektpositioner ej är tillräckligt robust för mätningar gjorda från de nya naturliga defekterna. Därför föreslås en tvådimensionell metod för denna estimering vilket bör ge betydligt mera robusta estimat eftersom en större mängd data används vid estimeringen.

Contents

List of Figures

List of Tables

1 Introduction

This report treats the ultrasonic measurements performed on the new V-welded carbon steel blocks and development of algorithms for feature extraction, flaw position estimation, etc. The software used below is partly based on the software used for immersion testing of simulated and artificial defects from the previous project *Ultrasonic Characterization of Defects* [1, 2, 3]. However, there has been a substantial rewriting of the algorithms, and new algorithms have also been added to fit the new contact measurements of the V-welded steel blocks. A substantial effort has also been put in complementary manual inspection related to interpreting the ultrasonic data obtained from the scanner. Section 2 describes the manufacturing of the new carbon steel blocks and the "natural" flaws that are implanted in them. The main part of the text, Section 3, describes the B-scan (and D-scan) measurements that have been performed and discusses the features found in the measurements. In Section 4 the algorithms for: position estimation, region of interest selection, feature extraction, and depth normalization are presented. This section also contains a discussion of the different defect classes proposed and a comparison of signal features between different flaw types. At the end of the section there is also a comparison of artificial flaws contra natural flaws. Finally, Section 5 gives a summary of performed work and Section 6 gives the conclusions.

2 Realistic Test Blocks

The first step of the project Ultrasonic Defect Characterization includes designing and manufacturing test blocks made of carbon steel (CS) containing realistic flaws in the weld. The original planning concerned 12 welded blocks, each with 3 flaws in the V-weld. After the discussion with the manufacturer (Sonaspection International Ltd.) the number of blocks has been reduced to four, mainly due to the substantial difference in production cost. Other important factor supporting this change was related to logistics in our laboratory which is not well prepared for handling heavy steel loads. It should be noted however, that despite the reduced number of blocks, the number of flaws has remained the same as planned, i.e. total 36 flaws of different types. Thus this change does not influence the extend of the experimental work. We decided to split block manufacturing in two steps, first to get CS blocks and then, after acquiring and processing ultrasonic data from the flaws, to manufacture similar blocks made of stainless steel (SS). The main reason for that is the need of practical experience before deciding what types of flaws should be manufactured in the SS blocks. However, the manufacturing of the SS blocks has been postponed for reasons which will be explained later in this report.

2.1 Description of the CS Test Blocks

Four blocks, each with 9 various flaws, were designed in collaboration with, and manufactured by Sonaspection International Ltd. All blocks have dimensions 42 mm $\times$ 400 mm $\times$ 600 mm and consist of two carbon steel plates, welded together (V-weld). The defect types and sizes manufactured in the blocks are summarized in Table 1. From Table 1 can be seen that our flaw population consists of 24 sharp flaws (various types of cracks and lack of fusion) and 12 soft type flaws (slag, porosity and over penetration). Closer analysis shows that we have three different types of cracks characterized by various sizes, angles and locations. The cracks were manufactured by mechanical fatigue and were implanted by semi-direct insertion (created before the welding process or at a pre-determined stage during welding). We have also natural sharp flaws in the form of lack of side wall fusion. This gives an idea of spread in the sharp flaw class which should also result in the variation of their ultrasonic signatures. On the other hand soft defects by their nature should result in similar ultrasonic responses, independent of their

Flaw Type	Size in mm	No of flaws	Abbreviations
Root Crack	3	3	RC
Root Crack	6	3	RC
Lack of Side Wall Fusion	3	3	LOF
Lack of Side Wall Fusion	7	3	LOF
Side wall crack	3	3	SWC
Side wall crack	7	3	SWC
Center line crack	3	3	CC
Center line crack	6	3	CC
Slag	3–6	3	S
Porosity	6–10	3	P
Over Penetration	3–5	3	OP
Lack of Penetration	2–25	3	LOP

Table 1: *Flaw list.*

location and size.

Sonaspection delivered detailed drawings of the blocks, as built flaw details and photographs of flaw signatures for each crack. Copies of Sonaspection block drawings are in Appendix B. A copy of the Sonaspection report was delivered to SKi. The test blocks have been subjected to careful ultrasonic inspected in our lab and all the defects were localized according to the reports from Sonaspection.

3 Test Block Measurements

This section describes the used transducers, the measurement setup, and the measurements performed.

3.1 Transducers

The contact UT inspection of the blocks has been performed using mechanized scanner and a digital ultrasonic system based on Saphir PC board. B-scans for each flaw were acquired and a flaw data base has been created.

Two miniature screw-in transducers from Panametrics, with center frequencies 2.25 MHz (type V539-SM) and 3.5 MHz (type A545S-SM) were used in the (shear wave) contact inspection: Both transducers had nominal element size 0.5" (13 mm) and were assembled by screwing

f_0 [MHz]	B [MHz] (-6dB)	Angle [Degrees]	Producer
2.25	89%	45	Panametrics
2.25	89%	60	Panametrics
2.25	89%	70	Panametrics
3.5	58%	45	Panametrics
3.5	58%	60	Panametrics
3.5	58%	70	Panametrics

Table 2: *Transducer list.*

directly into miniature angle beam wedges type ABWM-5T also from Panametrics. Six different

angle beam transducer configurations, listed in the Table 2 above, were created in this way. Advantage of this solution is quite obvious, by using the same active element we have obtained angle transducers with very similar characteristics. Since ultrasonic response of a particular flaw is determined both by the flaw type and by the transducer characteristics it is essential for defect characterization to keep transducer characteristic as constant as possible.

3.2 Measurement Setup

Four different scanning methods were used. The aim was to make direct measurements from the top side of the steel blocks shown in Figure 1a. However, for smaller angles direct measurements were obstacled by the upper surface of the V-weld. In such cases indirect measurements or measurements from the backside were performed instead, which is shown in Figure 1b and c. Another reason for making indirect (or backside) measurements was low amplitude of the

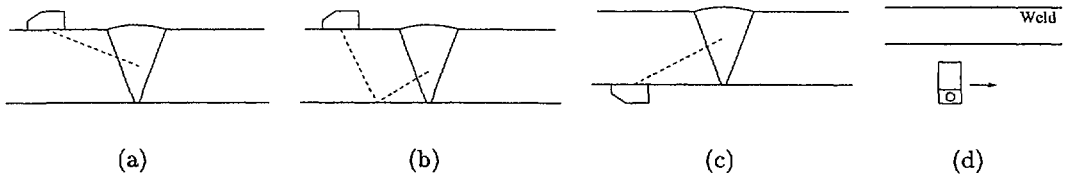

Figure 1: *(a) Direct measurements (b) Indirect measurements (c) Backside measurements (d) D-scan.*

reflection obtained in the direct measurement due to the angle between the transducer main beam and certain flaws, like sidewall cracks.

The fourth scanning method is shown in Figure 1d, which is so-called D-scans. That is, the probe is moved along the weld side-wise. D-scans are interesting because they reveal how the defect response varies along the defect. It is also interesting to see the response from the weld itself, both with and without a defect present. Typically the shape of the weld varies substantially spatially and D-scan shows this variation rather clearly.

3.3 Measurements

The performed measurements are displayed in Table 3 and Table 4. The measurements consist of B- and D-scan data matrices and the total number of measurements are 2×133. The main part of data comes from the welded steel blocks described above, but new measurements have also been performed, for comparison, on the two old aluminum blocks with artificial defects used in the previous project [3]. In addition to these measurements all flaws have also been investigated manually.

The artificial flaws in Table 4 named `SBH` are side-drilled holes, and the ones named `S` are cracks (notches).[1]

3.4 Results

In this section a number of B-scans from each defect type are shown for illustration. They are selected so that both common features and feature variations are represented for each defect type. Note also, that some of the images contain echos from non-defect parts of the weld, like the top

[1] For a more detailed description of the aluminum blocks see [3].

Defect	Direct			Indirect			Backside			D-scan		
	45	60	70	45	60	70	45	60	70	45	60	70
RC 1		•	•								•	
RC 2		•	•								•	
RC 3		•	•								•	
RC 4		•	•								•	
RC 5		•	•								•	
RC 6		•	•								•	
LOF 7					•		•	•			•	
LOF 8					•		•	•			•	
LOF 9					•							
LOF 10					•		•	•			•	
LOF 11					•		•	•		•		
LOF 12					•							
SWC 13					•		•	•	•		•	
SWC 14							•	•			•	
SWC 15					•		•	•			•	
SWC 16					•		•	•			•	
SWC 17				•			•	•		•		
SWC 18				•				•	•		•	
CC 19			•	•							•	
CC 20				•				•	•			•
CC 21				•				•	•		•	
CC 22				•					•			•
CC 23				•				•			•	
CC 24			•									•
S 25				•			•	•			•	
S 26				•				•	•		•	
S 27				•			•	•		•		
P 28				•			•				•	
P 29				•			•	•			•	
P 30				•			•	•		•		
OP 31		•									•	
OP 32		•									•	
OP 33		•									•	
LOP 34		•									•	
LOP 35		•	•								•	
LOP 36		•	•								•	

Table 3: *B-scan measurements made on the Steel-block welds with both 2.25 MHz and 3.5 MHz Transducers.*

Defect	45	60	Block
S 4–7	•		B1
S 7–4	•		B1
SBH 1	•		B1
SBH 2	•		B1
SBH 3	•		B1
S1	•	•	B2
S2	•	•	B2
S3	•	•	B2
S4	•	•	B2
S5	•	•	B2
S6	•	•	B2

Table 4: *B-scan measurements made on the aluminum blocks with artificial defects. The measurements were made with the 2.25 MHz and 3.5 MHz transducers.*

or bottom surface of the weld or the steel-weld junction. These echos are explained (if possible) when they are encountered. In the figure titles the name of the data files are given. An example is p28b 1 3 5, where p28 means porosity flaw 28, b means backside measurements, 1 indicates that the flaw is located in test block PL4501, and 3 5 is the used transducer frequency (3.5 MHz). The B-scans presented in the following subsections are from measurements with the 3.5 Mhz transducer. The reason for showing the 3.5 Mhz transducer only is that the measurements is performed on carbon steel blocks with very little material grain noise. This implies that the 2.25 MHz and the 3.5 MHz transducers should give similar results with the exception that the 3.5 MHz transducer has a higher center frequency and thus shorter wavelength and therefore higher resolution (both transducers has approximately the same bandwidth). There is, however, a comparison of the two transducers in Appendix A.

3.4.1 Center Cracks

The center cracks found in the steel test blocks can be either straight or slightly tilted. Figure 2 shows indirect measurements using the 45-degrees 3.5 MHz transducer. All echos around 60 mm stem from direct reflections from the bottom surface of the weld and all echos around 120 mm stem from indirect reflections from the top surface of the weld. One can see that there are two rather strong peaks (too strong to be diffraction echos) in all three B-scans. We can not find an unambiguous explanation for the presence of the second echos, but we believe that it must depend on the structure of the cracks implanted into the weld. These two peaks do not always occur in signals from center cracks, if we for example scan the defect in Figure 2a from the other side of the weld, we get only a single peak. This effect is also less pronounced if a higher angle probe is used. Figure 3 shows B-scans of the same defects obtained with a 60 degree transducer, and there is for example only one peak in Figure 3b (see Section 5 for a further discussion on this topic).

3.4.2 Sidewall Cracks

The sidewall cracks are located in the steel-weld junction and are therefore tilted with the same angle as the weld (30 degrees). This makes it difficult to apply direct measurements and all measurements are therefore performed from the backside or indirect. Figure 4 and Figure 5 show backside measurements performed with the 3.5 MHz 45- and 60-degrees transducers. All echos around 60 mm for the 45-degree transducer, and around 84 mm for the 60-degree

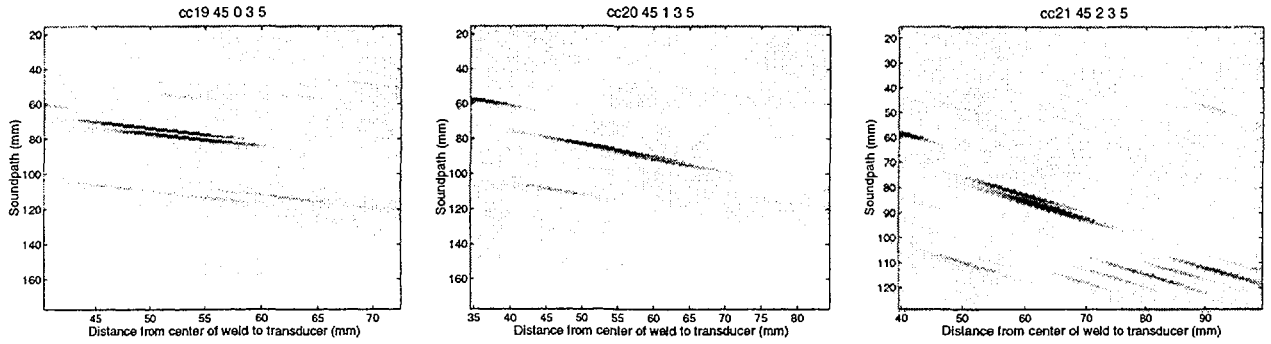

(a) (b) (c)

Figure 2: *Indirect measurements from center cracks using the 45-degrees 3.5 MHz transducer (a) 3 mm crack, 10 mm from bottom surface (b) 6 mm crack, 26 mm from bottom surface, tilted 2 degrees (c) 3 mm crack, 22 mm from bottom surface, 2 mm from center of weld, tilted 3 degrees.*

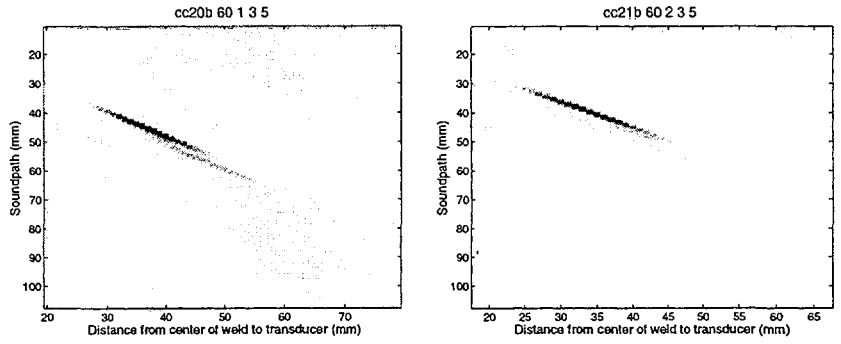

(a) (b)

Figure 3: *Backside measurements from center cracks using the 60-degrees 3.5 MHz transducer (a) 6 mm crack, 26 mm from bottom surface and tilted 2 degrees (b) 3 mm crack, 22 mm from bottom surface, 2 mm from center of weld, tilted 3 degrees.*

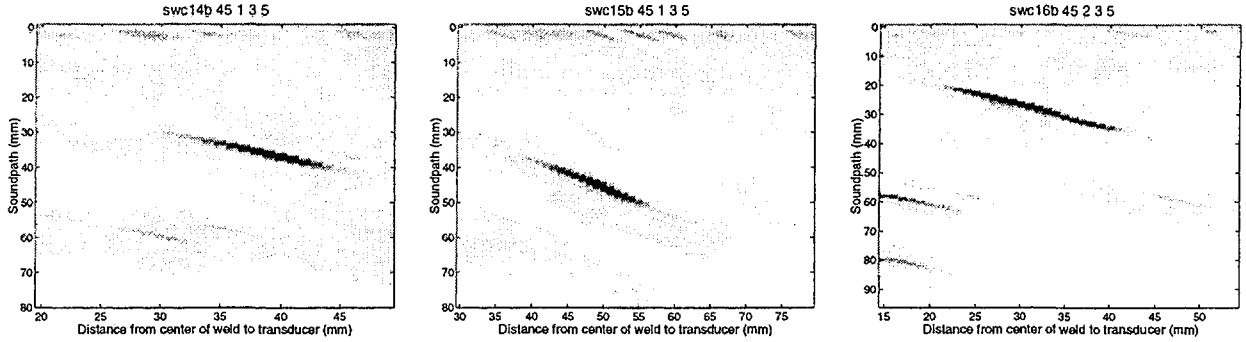

(a) (b) (c)

Figure 4: *Backside measurements from sidewall cracks using the 45-degrees 3.5 MHz transducer (a) 3 mm crack, 24 mm from bottom surface (b) 7 mm crack, 29 mm from bottom surface (c) 7 mm crack, 17 mm from bottom surface.*

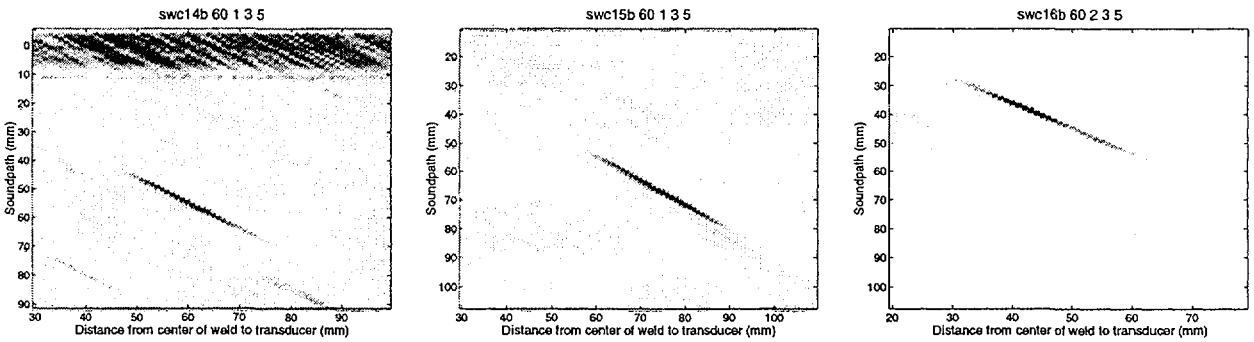

(a) (b) (c)

Figure 5: *Backside measurements from sidewall cracks using the 60-degrees 3.5 MHz transducer (a) 3 mm crack, 24 mm from bottom surface (b) 7 mm crack, 29 mm from bottom surface (c) 7 mm crack, 17 mm from bottom surface.*

transducer come from the top surface of the weld. No double echos, like for center cracks, are noted for the sidewall cracks.

3.4.3 Lack of Fusion

The lack of fusion (LOF) defects are located in the same way as sidewall cracks, and are therefore also tilted 30 degrees. This results in the same difficulty to make direct measurements here as well. Figure 6 and Figure 7 show measurements with the 45- and the 60-degree transducers, respectively. In the same way as for the previous backside measurements, echos around 60 mm

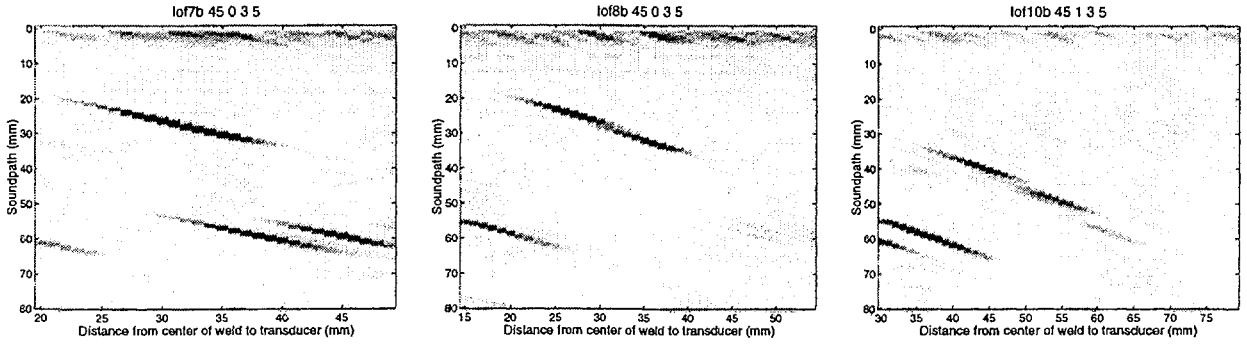

(a) (b) (c)

Figure 6: *Backside measurements from lack of fusion using the 45-degrees 3.5 MHz transducer (a) 2.9 mm crack, 23.5 mm from bottom surface (b) 6.9 mm crack, 29.4 mm from bottom surface (c) 6.9 mm crack, 17 mm from bottom surface.*

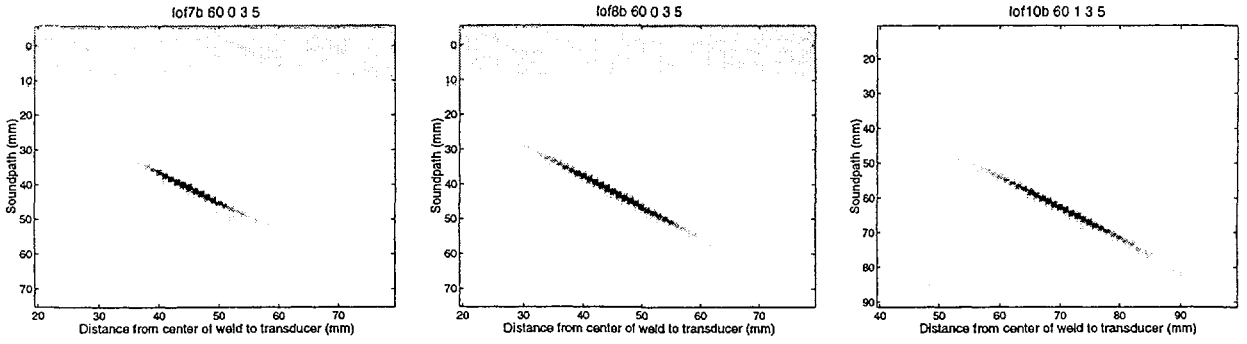

(a) (b) (c)

Figure 7: *Backside measurements from lack of fusion using the 60-degrees 3.5 MHz transducer (a) 2.9 mm crack, 23.5 mm from bottom surface (b) 6.9 mm crack, 29.4 mm from bottom surface (c) 6.9 mm crack, 17 mm from bottom surface.*

for the 45-degree transducer, and echos around 84 mm for the 60-degree transducer come from the top weld surface. Some of the LOF measurements have two peaks like the center cracks had (Figure 6b and c) for the 45-degree transducer, however they are more separated than for the center cracks. The double echos were only seen when the 45-degree transducer was used.

3.4.4 Slag

The echos from the slag inclusions are rather distinct regardless of which transducer that is used. Figure 8 and Figure 9 show four examples using the 45- and 60-degree transducers. No direct measurements were performed because of practical reasons (the transducer is obstacled by the weld surface), see Section 3.2.

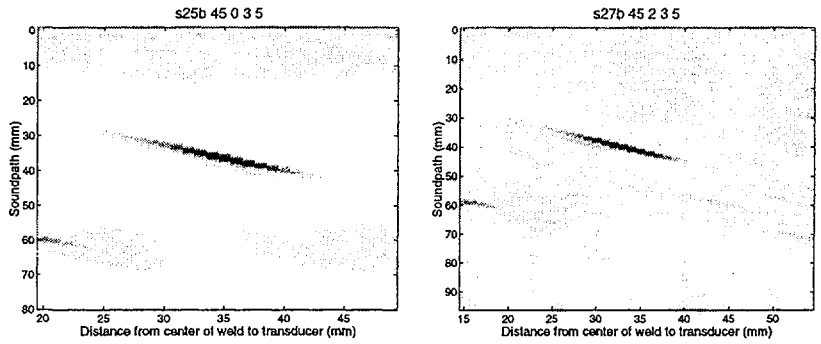

(a) (b)

Figure 8: *Backside measurements from slag using the 45-degrees 3.5 MHz transducer (a) 3 mm slag, 25 mm from bottom surface (b) 5 mm slag, 26 mm from bottom surface.*

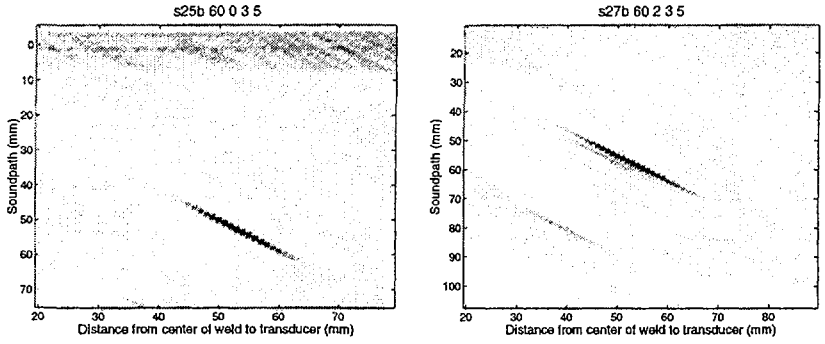

(a) (b)

Figure 9: *Backside measurements from slag using the 60-degrees 3.5 MHz transducer (a) 3 mm slag, 25 mm from bottom surface (b) 5 mm slag, 26 mm from bottom surface.*

3.4.5 Porosity

Porosity can rather easily be separated from other types of defects due to the multiple echos encountered in the ultrasonic signal. Figure 10 and Figure 11 show 6 examples of B-scans acquired using both the 45- and 60-degree transducer from backside measurements. The echos observed at approximately 60 mm (and 84 mm) are, as usual, from the top surface of the weld. Note that the echos at approximately 25 mm in Figure 10c and 40 mm in Figure 11c probably come from a rather strong reflection of the steel-weld junction present in test block PL4503.

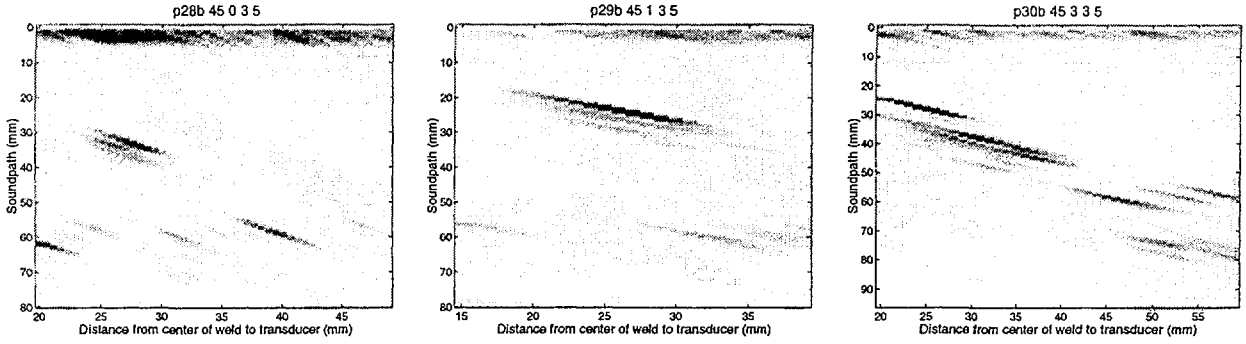

(a) (b) (c)

Figure 10: *Backside measurements from porosity using the 45-degrees 3.5 MHz transducer (a) 6 mm porosity, 22 mm from bottom surface (b) 8 mm porosity, 15 mm from bottom surface (c) 9 mm porosity, 26 mm from bottom surface.*

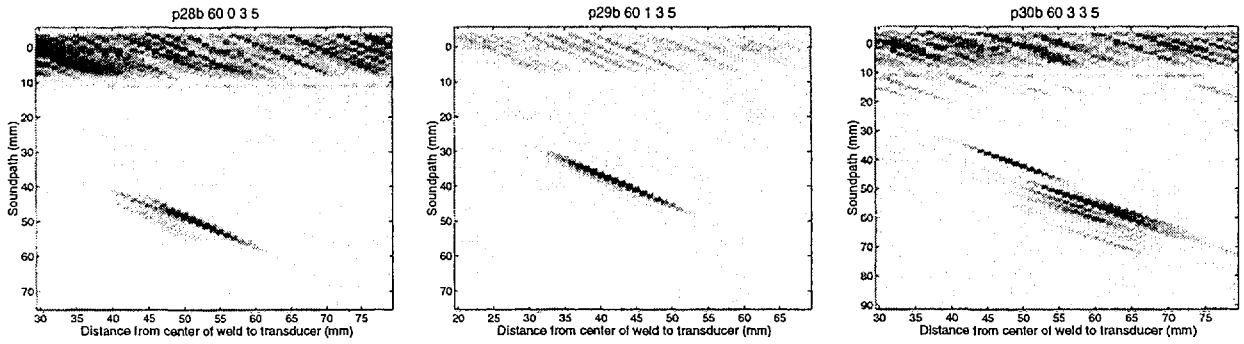

(a) (b) (c)

Figure 11: *Backside measurements from porosity using the 60-degrees 3.5 MHz transducer (a) 6 mm porosity, 22 mm from bottom surface (b) 8 mm porosity, 15 mm from bottom surface (c) 9 mm porosity, 26 mm from bottom surface.*

3.4.6 Root Crack

Root cracks result in strong reflections from the crack-bottom surface corner. In some cases, a small echo from the crack itself appears slightly before the crack-bottom echo. This "pre-echo" might be seen in the B-scans presented in Figure 12 and Figure 13, but will be more easily seen in A-scans presented later in Section 4.2.2. The origin of this type of echos is some what

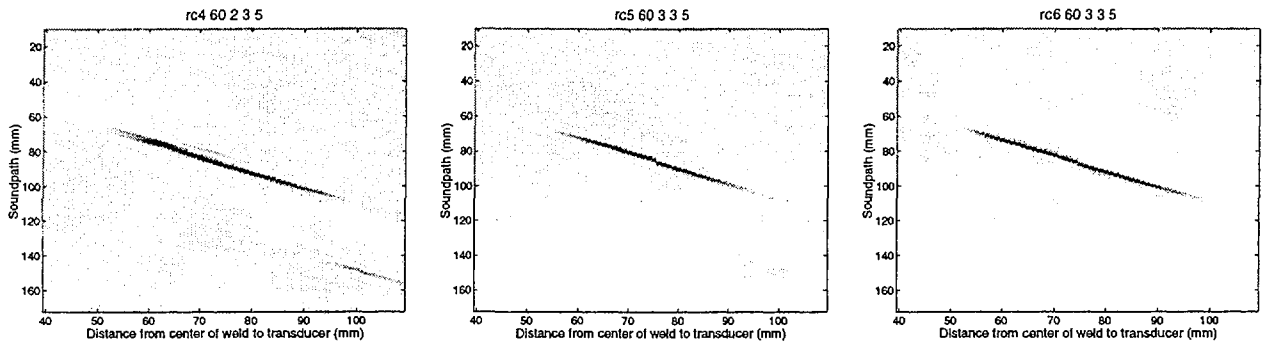

(a) (b) (c)

Figure 12: *Direct measurements from root cracks using the 60-degrees 3.5 MHz transducer (a) 3 mm crack, tilted 3 degrees (b) 3.4 mm crack, tilted 17 degrees (c) 7 mm crack, tilted 27 degrees.*

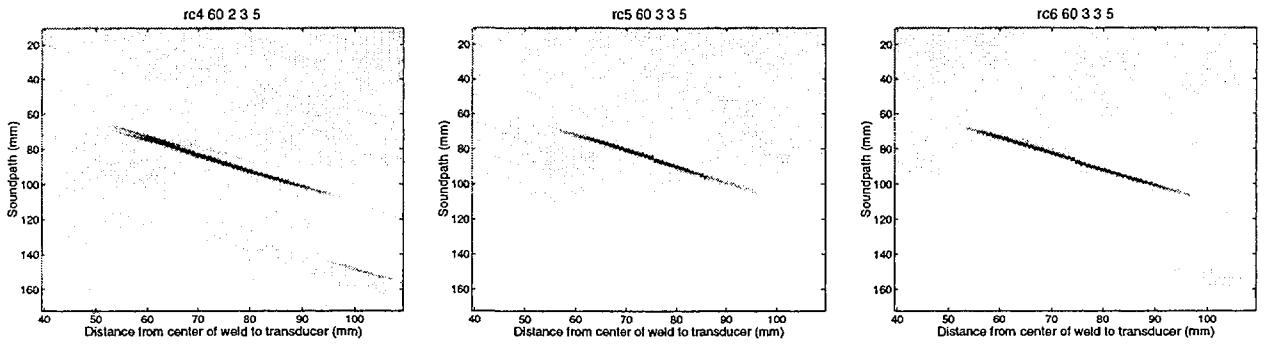

(a) (b) (c)

Figure 13: *Direct measurements from root cracks using the 60-degrees 3.5 MHz transducer (a) 3 mm crack, tilted 3 degrees (b) 3.4 mm crack, tilted 17 degrees (c) 7 mm crack, tilted 27 degrees.*

unclear, but it can be due to the same phenomena as the double echos encountered in the signals for the center cracks.

3.4.7 Lack of Penetration

The echos from lack of penetration defects looks rather similar to root cracks, but they are more "distinct" since there is no echo from the top parts of the defect, only echos from defect-

bottom surface corner is present. Figure 14 and Figure 15 show four examples using the 60- and 70-degree transducers (from direct measurements).

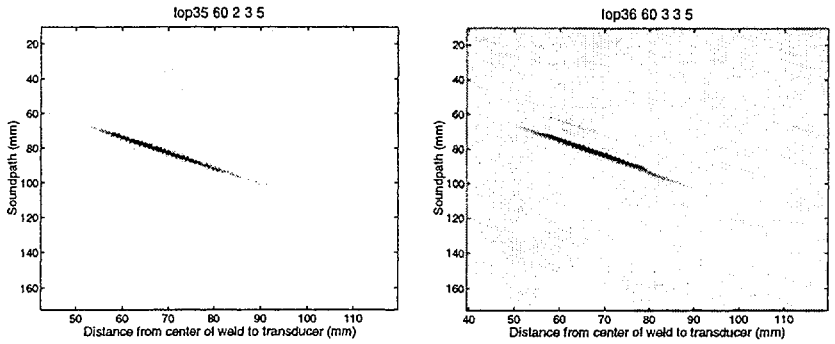

(a) (b)

Figure 14: *Direct measurements from lock of penetration using the 60-degrees 3.5 MHz transducer (a) 2 mm lack of penetration (b) 2.5 mm lack of penetration.*

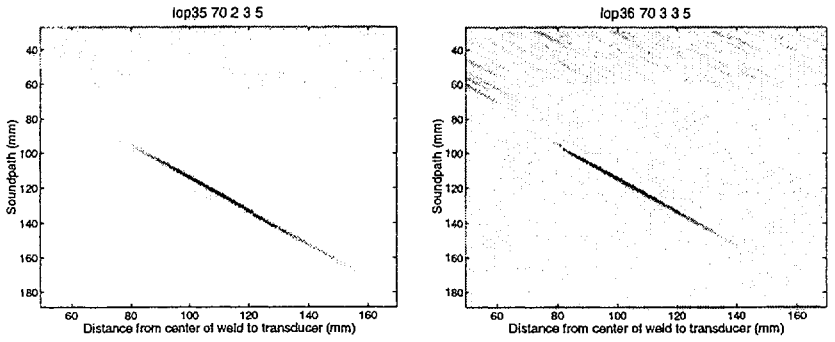

(a) (b)

Figure 15: *Direct measurements from lack of penetration using the 70-degrees 3.5 MHz transducer (a) 2 mm lack of penetration (b) 2.5 mm lack of penetration.*

3.4.8 Over Penetration

Over penetration can rather easily be distinguished from root cracks and lack of penetration since it is characterized by a proportionately long tail of small pulses after the main pulse which comes from the bottom weld surface. Figure 16 shows three examples.

3.4.9 D-scans

D-scans gives information of how the response signal varies along a flaw. Particularly one can estimate the length (side-wise) of the flaw from these type of measurements. Two examples of D-scans are shown in Figure 17. Note the response from the bottom weld surface—shown as a horizontal line trough the B-scan—and how it is "shadowed" by the root crack in Figure 17a.

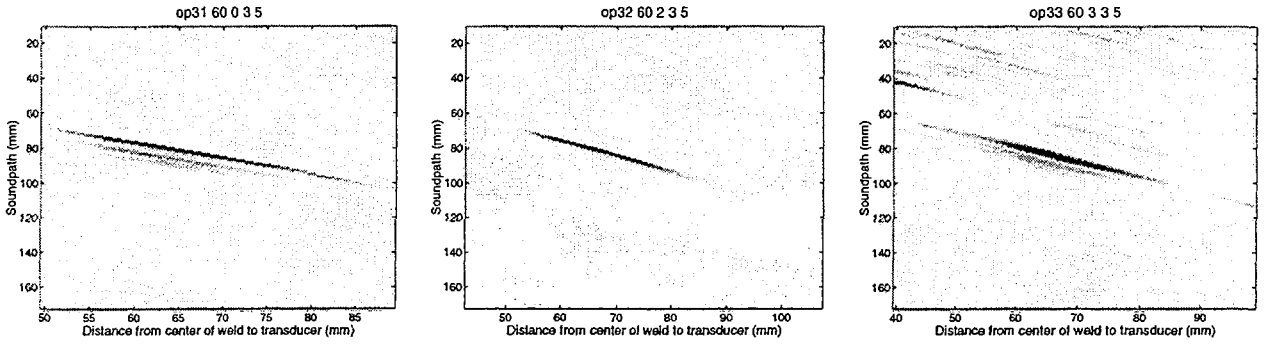

(a) (b) (c)

Figure 16: *Direct measurements from over penetration using the 60-degrees 3.5 MHz transducer (a) 3 mm over penetration (b) 4.5 mm over penetration (c) 5 mm over penetration.*

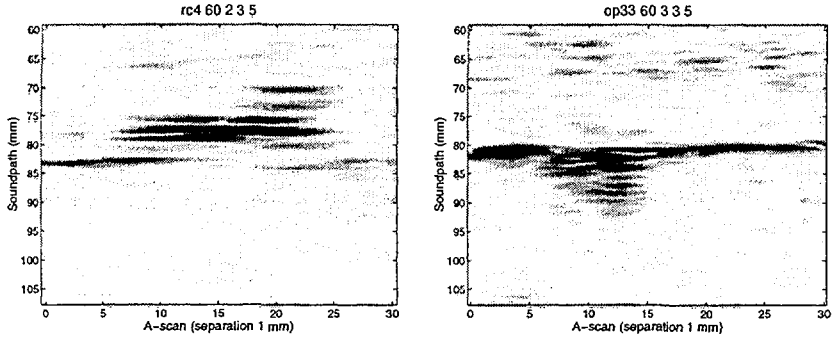

(a) (b)

Figure 17: *D-scans (a) 3 mm root crack (b) 5 mm over penetration.*

Note also the typical ringings after the weld surface response in Figure 17b that are characteristic for the over penetration type of flaws.

4 Defect Characterization

4.1 Signal Features and Feature Extraction

4.1.1 Pre-processing

Currently, like in the previous study [1, 2, 3], we only look at the envelope of the collected ultrasonic B-scan data. The envelope is calculated by means of the Hilbert transform. The resulting data is also smoothed with a low-pass filter to reduce the measurement noise present in data.

4.1.2 Finding Position of Defects

The flaw position is used for both region of interest (ROI) selection and depth normalization, and it is therefore important to have accurate and robust position estimates. The current method to find the flaw position is based on fitting an hyperbolic function to the flaw response in B-scan data, see [2]. This method is summarized below:

> The curves formed by a point scatterer in a B-scan, obtained with the contact measuring setup in Figure 1a–c, are shaped as a part of an hyperbola given by the equation
>
> $$r = \sqrt{x_{transd}^2 + z_{flaw}^2}. \tag{1}$$
>
> The position estimate $(\hat{x}_{transd}, \hat{z}_{flaw})$ is found by minimizing the summed squared error $\sum_i \parallel r_{max}^{(i)} - \hat{r}^{(i)} \parallel^2$, $i = 1, 2, \ldots, N$, for a selected number of A-scans, where $r_{max}^{(i)}$ is the position of the max amplitude of the envelope of the ith A-scan.

Another approach, which would be more robust is to fit a 2D-function (surface) to the flaw response signal. Such a function would approximate the flaw response in a more unambiguous way than than the hyperbolic contour defined by Eq. (1). It would be more robust since many points of the 2D response would be used for its estimation. Or re-phrased, we use a flaw model, and adjust the parameters of this model so that a synthetic B-scan generated from this model is as similar as possible to the original measured B-scan. One of the parameters of this model would then be the position of the flaw, which is exactly what we are searching for.

4.1.3 ROI Selection

Selection of region of interest (ROI) is not a trivial task for the type of ultrasonic images obtained from the "real" flaws encountered here. Ideally we would like to position an hyperbolic shaped analyzing window around a flaw response signal in an B-scan image. The position of the window should be determined based only on the (exact) position of the flaw. The problem is that the defect position is unknown and we have to estimate it, as mentioned in the previous section. However, this estimation is not accurate enough for the precise positioning required here. In the previous reports [2, 3] the echo-dynamics (max amplitude variation) of the flaw response was used for the positioning. Figure 18 shows two examples of echo-dynamics. As one can see the echo-dynamics curves can be skew, have more than one peak, etc. If the B-scan has two

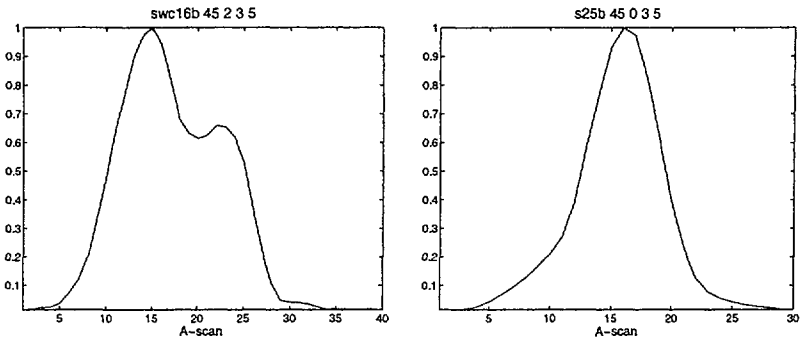

(a) (b)

Figure 18: *Echo-dynamics from (a) a sidewall crack and (b) a slag inclusion.*

(or more) separate peaks, like in Figure 2a, the situation becomes even more complicated. In the previous report, mentioned above, the echo-dynamics was smoothed with low-pass filtering which partially solves the problem, and this worked well for the simulated and artificial defects encountered there. Experiments have also been made with using center-of-mass calculations, but this approach is sensitive to long tails with high amplitude (energy) in the echo-dynamics. Therefore, we have currently adopted and used the same algorithm as before. This algorithm can be summarized as follows:[2]

1. Low-pass filter the echo-dynamics.
2. Find position of max amplitude of the filtered echo-dynamics.
3. Select a number n of A-scans centered around this position. The number n depends on the depth of the defect, which is described later in Section 4.1.6.

4.1.4 Classical Features

Perhaps, most commonly used features for classification of defects during ultrasonic testing is the rise time, pulse duration and fall time. These three features are calculated from the times depicted in Figure 19. Typically one uses the 90% and 10% levels for the calculation, but here

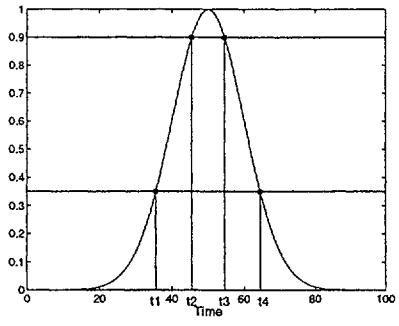

Figure 19: *The four times used for calculating rise time, pulse duration and fall time.*

[2]ROI selection can probably also, like position estimation, gain accuracy if we introduce a flaw model.

the same levels as in [3] (90% and 35%) are adopted to avoid problems with noise.

When 2D data are available (B-scans) one commonly uses the echo-dynamics (see previous section) which gives a description of the amplitude variation between consecutive A-scans in a B-scan.

The basic features described here all rely on a rather well defined pulse in order to get reliable results. Smoothing (low-pass filtering) solves some of the problems with noise, for example, but some problems remain. Figure 20 shows the envelope of A-scans from three different types of defects. In spite of the very different shape of the waveforms, the rise time, pulse duration and

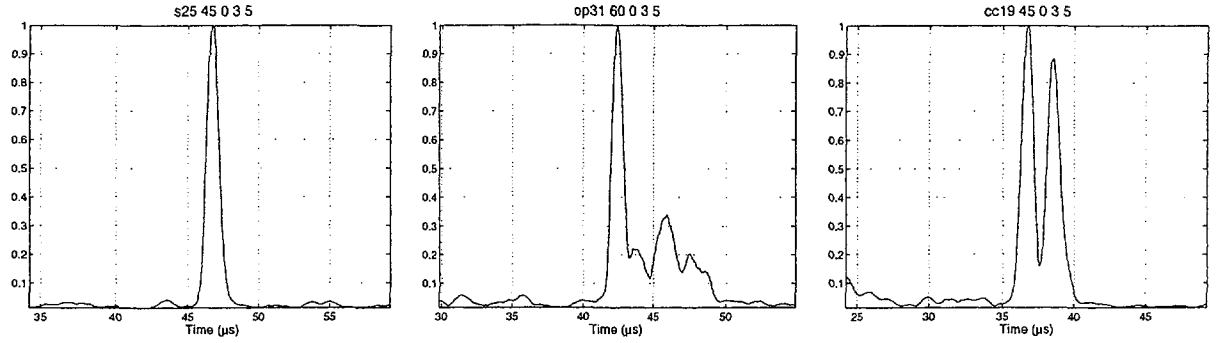

(a) (b) (c)

Figure 20: *Envelope of A-scans from three different flaws (a) Slag inclusion (b) Over penetration (c) Center crack.*

fall time are rather similar for all of the signals in Figure 20. It is evident that more powerful features are needed if the classification should be feasible for the natural flaws encountered here.

4.1.5 Feature Extraction using the Discrete Wavelet Transform

The *discrete wavelet transform* (DWT) forms an orthonormal basis which has several interesting features for this application. The basis functions are impulse-like functions very suitable for modeling the pulses in ultrasonic signals. If an analyzing window is centered around an ultrasonic pulse, we can examine at which position and scale this pulse has significant energy, which is reflected in the wavelet coefficients given by the DWT.

The basis functions in the DWT consist of local functions with different positions and scales [4]. All basis functions are constructed from the same template function, called *mother wavelet*, using the following formula

$$\psi_{j,k}(t) = 2^{j/2}\psi(2^j t - k) \qquad t = 1, 2, \ldots, N \tag{2}$$

and we can express any function f as a linear combination the basis functions

$$f(t) = \sum_{j,k} w_{j,k}\psi_{j,k}(t). \tag{3}$$

The wavelet coefficients are given by the inner product

$$w_{j,k} = \langle f, \psi_{j,k} \rangle. \tag{4}$$

It should be noted that the envelopes of typical ultrasonic signals can be well described with only a few of the large scale components (wavelets), which result in a good data compression ability.

There are several different types of pre-defined mother wavelets available in common software packages, like the Wavelet toolbox for MATLAB. Figure 21 shows the first (largest scale) basis functions of the *Coiflet 2* mother wavelet, which is a fairly smooth wavelet suitable for this application. In Figure 22 the echo-dynamics and the first 16 DWT coefficients from the same

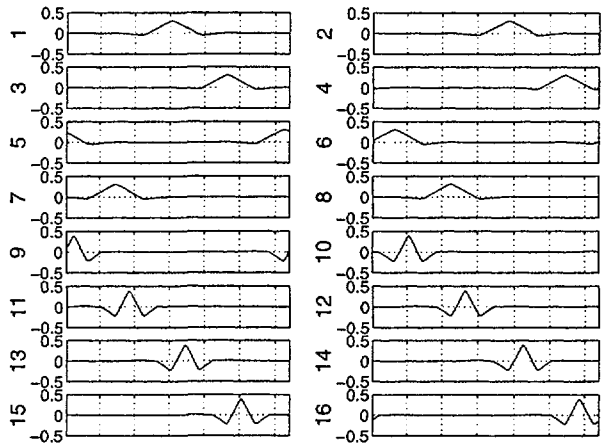

Figure 21: *The first 16 basis functions of the Coiflet 2 mother wavelet.*

A-scans are displayed. One can clearly see how the echo-dynamics is reflected in the wavelet

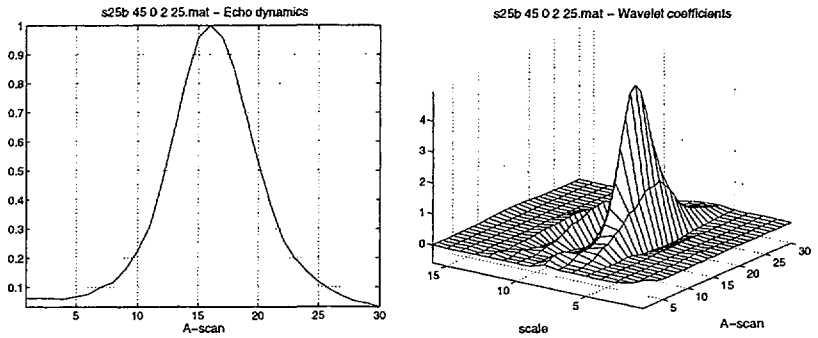

(a) (b)

Figure 22: *(a) The echo-dynamics from a slag inclusion. (b) The first 16 wavelet coefficients from the same A-scans as on (a).*

coefficients.

4.1.6 Depth Normalization

In an ultrasonic B-scan, a defect located close to the transducer will be seen in a fewer A-scans than a similar defect present further away from the probe, due to the lobe characteristics (cone-beam geometry) of the probe. If we look at the echo-dynamics from two flaws at different depths, the flaw closest to the transducer will have a narrower shape than the other flaw. A simple way to normalize is to re-sample the echo-dynamics (or wavelet coefficients) in some angle interval. That is, the feature vector (or matrix) is re-sampled in an angular scale instead of the original linear scale (Cartesian coordinate system). Figure 23 shows a defect and probe positions given

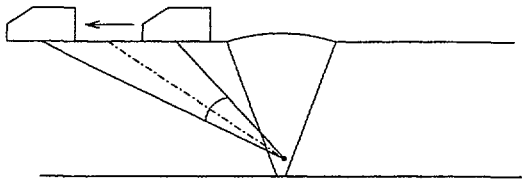

Figure 23: *Probe positions seen from a defect in a given interval of observation angle.*

for fixed angle interval. The depth normalization procedure consists in re-sampling the features for a suitable angular interval given the depth of the flaw. This implies interpolating features from flaws located close to the probe, and down sampling features for flaws that lie further away from the probe. The position of the flaw is calculated in the same way as in Section 4.1.3.

Using this normalization technique we implicitly assume a rather idealized probe model, that is, we ignore side lobes and we assume that the probe lobe is rather symmetric and that the material has a unity transfer function. A more sophisticated and more computationally intensive approach would be to measure the characteristics of the probe more carefully, for example, from side drilled holes at different depths. Then, the spatial probe characteristics could be de-convolved from the measured ultrasonic response, resulting in a pure flaw response signal.

4.2 Defect Classes

When comparing the available data from the different types of real defects, one realizes the complexity of the task. The variability of ultrasonic responses from the same type of defects seems rather large and one has to be very careful to pin-point the right reflector causing the particular echo. For example, an echo from the steel-weld junction can easily be interpreted as an defect.

A realistic goal here is to categorize defects in sharp defects, like cracks and lack of fusion, and volumetric (or soft defects), like porosity and slag inclusions. Defects in the bottom of the weld are also easy to distinguish from other flaws since they all occur at the same position. Therefore, the flaw types are divided in three main groups which are crack-like defects, volumetric defects, and defects in the bottom of the weld.

4.2.1 Crack-like Defects and Volumetric Defects

The Figures 24–27 show envelopes of A-scans and echo-dynamics for crack-like defects and volumetric defects. By studying these type of figures and B-scan images one can make at least two observations:

- The ultrasonic responses from crack type defects exhibit a large variation of features. This is especially clear for center cracks and lack of fusion defects.
- It is very difficult to distinguish between sidewall cracks and slag inclusions.

Expressed in pattern recognition terms we have large within-class variation for cracks and overlapping class regions between slag inclusion and SWC:s. Porosity is the type of defect that is easiest to separate from the other classes, due to the multiple echos which this type of defects produce.

One conclusion from these measurements is that we need a rather large number of examples from crack type of defects in order to see so many variations as possible. Another conclusion is

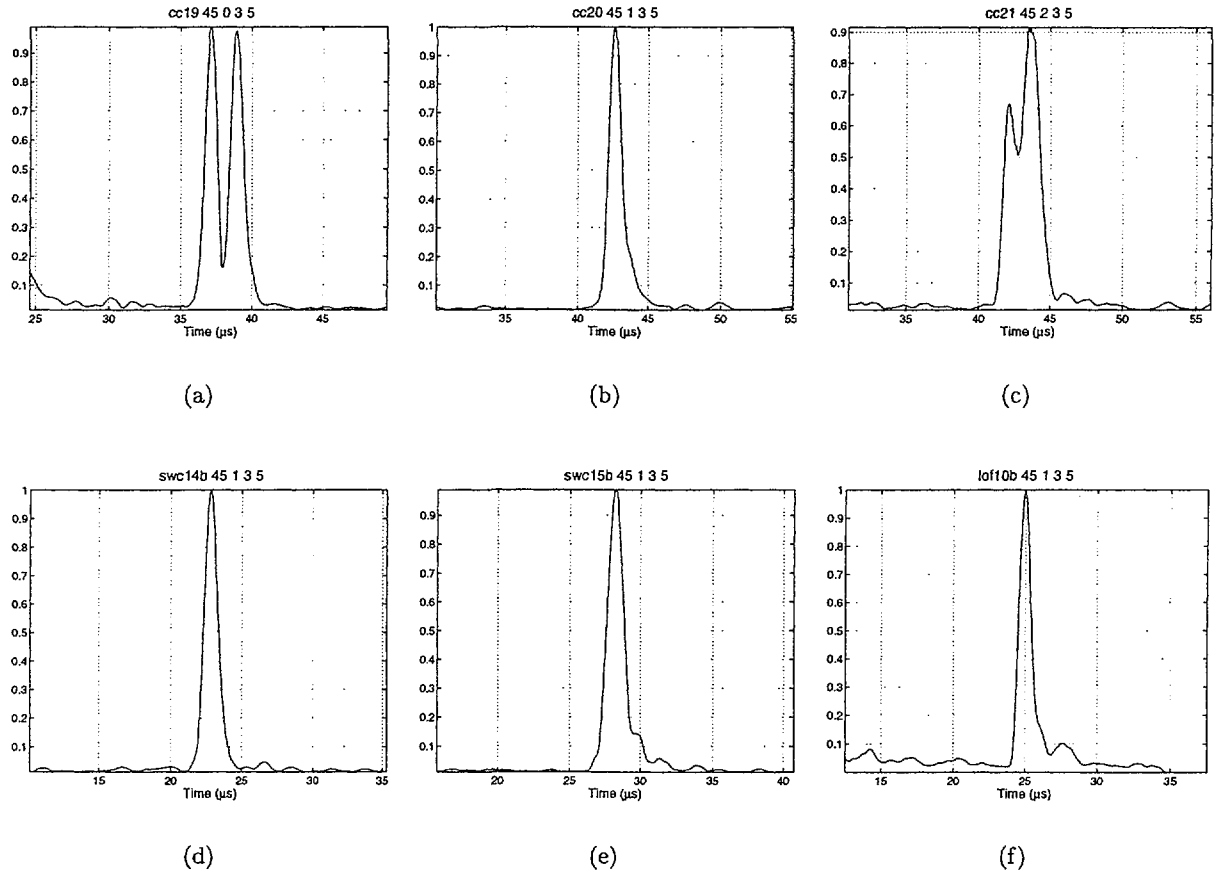

Figure 24: *Envelope of A-scans from crack-like defects. (a)-(c) Center cracks (d)-(e) Sidewall cracks (f) Lack of fusion.*

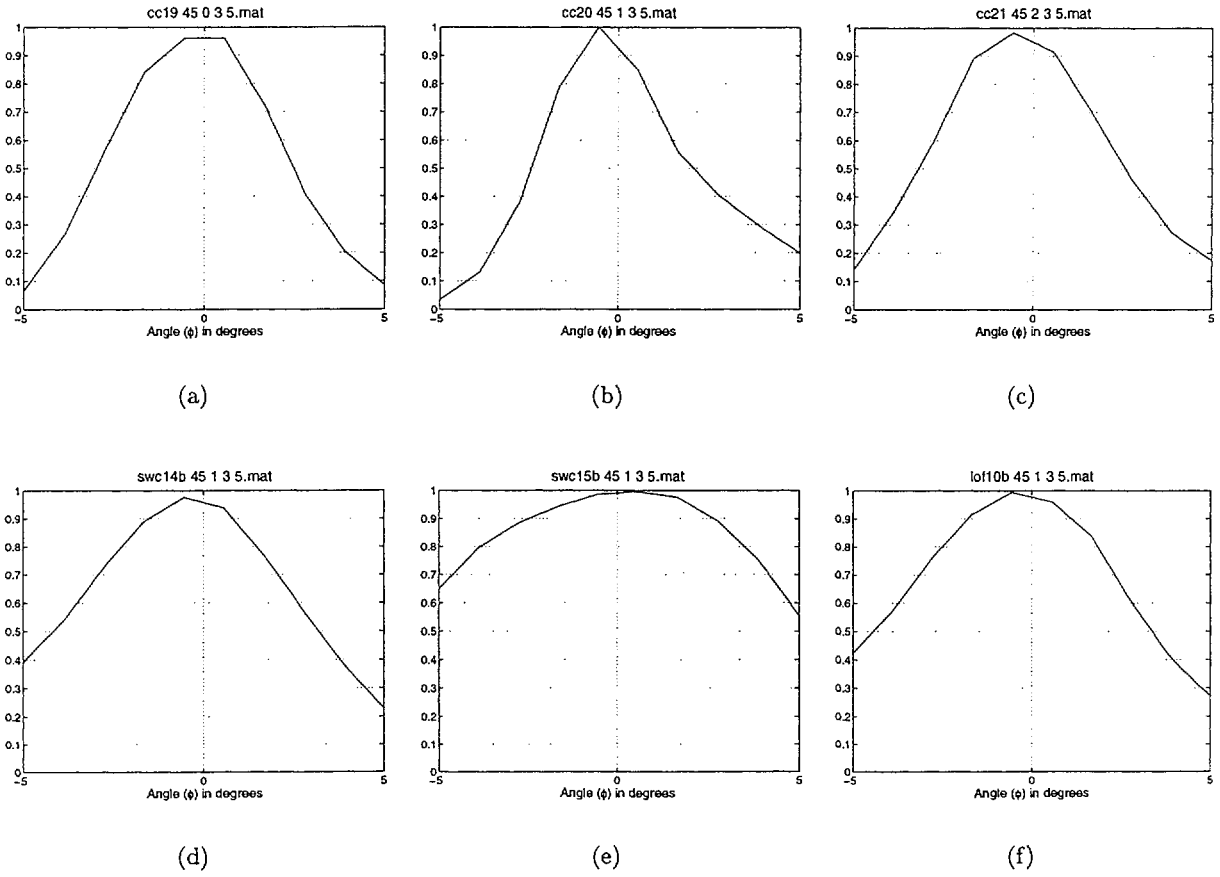

Figure 25: *Echo-dynamics in the angle range -5 to 5 degrees from crack-like defects. (a)-(c) Center cracks (d)-(e) Sidewall cracks (f) Lack of fusion.*

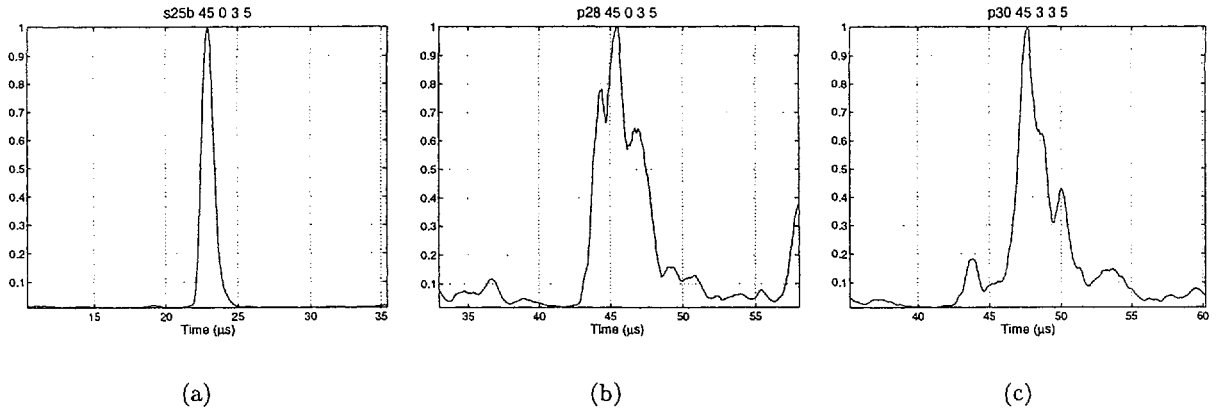

Figure 26: *Envelope of A-scans from volumetric defects. (a) Slag inclusion (b)-(c) Porosity.*

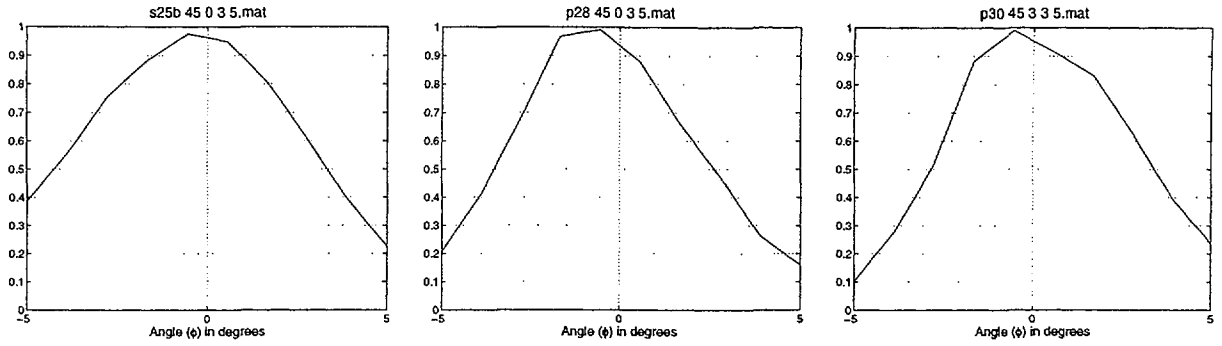

(a) (b) (c)

Figure 27: *Echo-dynamics in the angle range -5 to 5 degrees from volumetric defects. (a) Slag inclusion (b)-(c) Porosity.*

that it seems to be very difficult to use the classical type of features as described in Section 4.1.4. That is, more sophisticated tools are needed and using the discrete wavelet transform is an interesting option.

4.2.2 Defects at the Bottom of the Weld

The defects located at the bottom of the weld include three types of flaws: over penetration, lack of penetration, and root cracks. Figure 28 shows one example of each type. The within-class

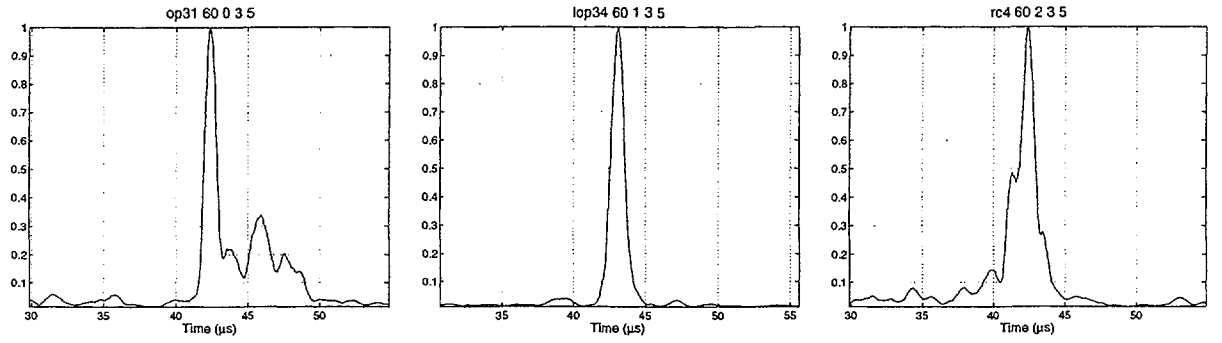

(a) (b) (c)

Figure 28: *Envelope of A-scans from Defects in the bottom of the weld. (a) Over penetration (b) lack of penetration and (c) root crack.*

variation seems to be much smaller for the defects at the bottom of the weld than for the types cracks described in Section 4.2.1. The class separation between the three different flaw types also looks larger than the former case. Lack of penetration has a rather "clean" pulse shape, over penetration has typical ringings after the main pulse, and root cracks result often in a pulse which comes slightly before the main pulse, which is rather clearly seen in Figure 28c.

With classical features we might be able to separate the three flaw types. That is, if the ringings of the over penetration and the "pre-pulse" of the root cracks are not separated too far

from the main pulse. A large separation between the ringings (or pre-pulse) and the main pulse will result in that only the main pulse is used for feature extraction. In fact, the pre-pulse or ringings might not even have a pulse amplitude that is higher than lower limit, which results in a total loss of these features.

However, if the DWT is used we preserve full information about the exact pulse shape and there is no risk of loosing information of low amplitude pulses as long as they occur inside the analyzing window.

4.3 Natural Contra Artificial Defects

As mentioned earlier B-scan data were also collected for the aluminum blocks with artificial defects used in the previous reports. Figure 29 shows a B-scan from block B1 were four artificial cracks (notches) are located. The cracks have a depth of 2 mm, 4 mm, 4 mm and 8 mm (from

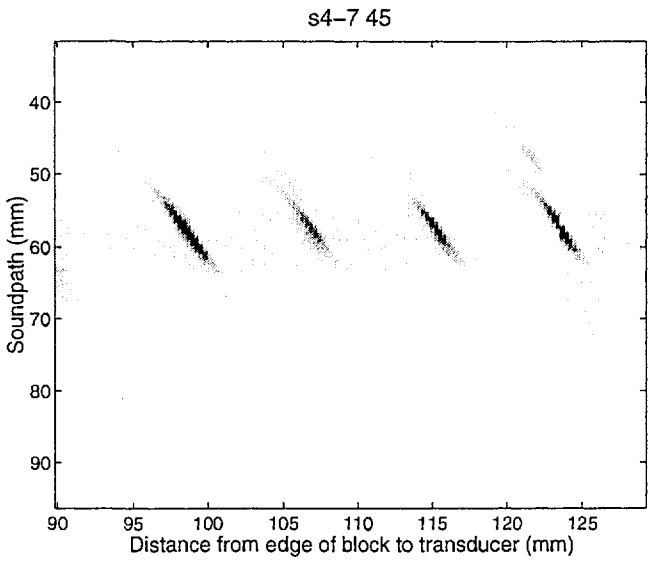

Figure 29: *Four artificial cracks (notches) in the B1 aluminum block.*

left to right in the figure). One can clearly see the diffraction echos, whose location in the B-scan is in agreement with the size of the defects. Figure 30 shows one A-scan (and the envelope) from the same B-scan as in Figure 29. The pulse shape from the artificial defects are very "clean" compared to the ones from the steel blocks with real defects above. There are no double echos or irregular pulse shapes present in the signals from the artificial cracks in the aluminum data, as was the case for the real crack signals from the steel blocks. The defect characterization (i.e. classification) task becomes much simpler since the within-class variation is much lower than for real flaws. An implication of this is that the number of data needed "to span" the room of possible flaw signals is much lower for artificial defects than for the real defect counterpart. The features needed for classification are also simpler, echo-dynamics, rise time, pulse duration and fall time work well for artificial defects as shown in report [3], in contrary to the real flaw signals were more sophisticated features are needed, as described above.

5 Summary of Performed Work

To begin with, all defects have thoroughly been investigated manually using hand hold probes. This was done in order to gain experience before a database of B- and D-scans were created.

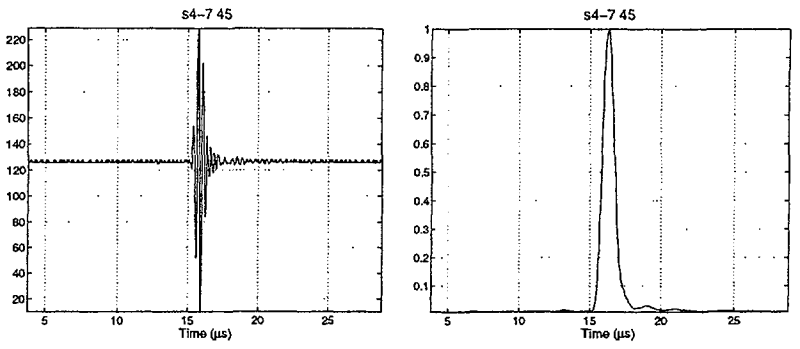

(a) (b)

Figure 30: *One A-scan from a crack (notch) in aluminum block B1. (a) A-scan and (b) Envelope of the same A-scan.*

Based on experience from the manual inspection, B- and D-scan measurements where then performed using suitable transducers and transducer wedges. In addition to the carbon steel block measurements additional measurements have also been performed on artificial defects in an aluminum block.

The ROI selection and feature extraction algorithms which previously were made for immersion measurements on aluminum blocks have been substantially re-written to 1) fit the new carbon steel block measurements, and 2) to make it possible to incorporate new more powerful feature extraction techniques.

The measurements were then divided in three groups, volumetric (soft) defects, sharp defects (eg. cracks), and defects at the bottom of the weld. The measurements from these groups where then compared using: raw data, traditional features and the linear discrete wavelet transform. Additionally, the CS measurements were also compared to the data from the artificial defects in the aluminum block and simulated data from the UT-Defect program [2, 5].

A substantial effort have been made on determining the origin of the double echos which were encountered in some of the measurements. It turned out to be very difficult to explain the phenomena based only on the measurements made using the techniques described in previous sections. One possible explanation of this is though, that the extra echos comes from structures in the weld which is due to the manufacturing of the artificial defects. In order to make measurements with normal (0°) probes possible, one block was then send to an mechanical workshop were the upper weld surface was machined off. Examining the measurements performed with a normal probe on, for example, center cracks resulted in strong reflections which normally should not have been present. One could expect diffraction echos but such echos are several orders of magnitude lower than the echos encountered here. The most likely explanation is that the reflection echo originates from implanted material (coupon) containing the crack. It is worth noting that the coupon would not be detected by the radiographic examination due to unfavorable angle of the beams.

The final conclusion is that the double echos must be regarded as abnormal and hence not representative as "real cracks". However, regarding the remaining defects, we still can see a larger variation in data than that for the artificial and simulated data.

Due, to the high signal variability no immersion measurements have been performed. The reason for that is, obviously, that we need a number of enhancements to the signal processing tools before it is reasonable to acquire data from more difficult measurement situations, that is,

from immersion testing or from measurements of SS blocks.

6 Conclusions

During the evaluation of ultrasonic data acquired from the V-welded steel blocks it became evident that the characterization task is much more complex than for the former simulated and artificial flaw signals. For example, in a V-weld there are other reflectors than flaws that result in ultrasonic pulses, like the top and bottom weld surfaces and steel-weld junctions. The feature space of possible flaw signals is also considerably larger for the real defects than for the artificial counterpart. That is, the variation of the ultrasonic signals from one type (class) of defects is much larger for real than for artificial defects.

Our goal is to separate soft (or volumetric) defects from the sharper ones (crack-like), but if one studies the echo-dynamics and the pulse shapes (i.e. the envelope) of slag inclusions and side wall cracks it becomes apparent that they are very hard to separate. This implies that we might encounter overlapping feature regions—especially if we only use classical features like fall/raise times, pulse duration and echo dynamics. This is exemplified in Figure 31 where a fictitious example characterized by only two features is shown. In this figure there are three

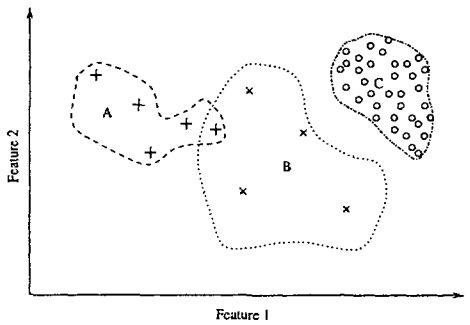

Figure 31: *A fictitious two feature example.*

classes present: one labeled A (with dashed boundary), and one B (with dotted boundary) and finally class C (with dash-dotted boundary). There is also a number of examples from each class shown in the figure, where the ×:es are from class A, the +:es from class B, and the ○:es are from class C. As one can see class A and B are overlapping and they also have a low number of examples which makes it very difficult to design a classifier with a proper decision boundary. Class C exemplifies the desired case with a sufficient number of examples and non-overlapping class boundaries. To avoid this overlapping class boundary scenario, more powerful feature extraction algorithms are needed to achieve feasible classification performance.

High variation of the ultrasonic signals from the V-weld has also two further consequences: flaw position estimation can be poor (if the B-scan contains several peaks for example), and the amount of data needed to construct a reliable classifier is large.

Below, we list a number of conditions that must be fulfilled for a successful classifier

- Ensure that the measurements are good (informative) enough to distinguish between different types of defects. This is vital, because we can of course not expect to be able to distinguish between different defects if the information needed is not present in the measurements.
- Representative features. The features that are fed to the classifier must preserve the information needed for successful classification.

- A sufficient number of examples. As a rule of thumb one needs at least ten times as many examples as the parameters in the classifier, that is, to avoid that the classifier learns the training examples and performs poor on unseen examples. Moreover, we need enough representative examples to span the whole room of possible flaw signals for each defect class. If the last condition is not fulfilled we get a classifier which is not able to classify all defect signals properly.

The second condition is clearly not fulfilled with classical features and we must, therefore, utilize more powerful methods. Examples of such methods are: wavelet analysis, principal component analysis (PCA) [6] and independent component analysis (ICA) [7]. The last two examples are interesting since the basis functions used are completely determined from data. The first condition might not be fulfilled with a single B-scan measurements only. A common practice in such situations when it is difficult to categorize a measurement is to combine measurements from several transducers (with different angles, center frequencies etc.) and TOFD measurements. This technique is usually known as *data fusion*. The last condition is more cumbersome. Clearly we do not have, and can not expect to have a sufficient number of examples to span the whole room of possible flaw signals, which is huge since we must account for different orientation, flaw size, crack roughness etc. Therefore, one could not expect to obtain a feasible classifier with this low amount of data using a standard pattern recognition approach. Hence, we have to incorporate more knowledge, apart from the knowledge we obtained by looking at examples of ultrasonic data corresponding to available defects. Such knowledge can, for example, take form of expert knowledge of an experienced operator or the form of a flaw model. The simulated and the artificial data (Section 4.3) showed a much lower signal variation than the real counterpart, and could therefore not be used to gain more training data. However, incorporating a model can still supply us with some very valuable knowledge, like flaw position and perhaps flaw orientation. This knowledge would be very valuable for locating ROI, classification and normalization.[3]

To sum up the conclusions; we deal with a complex classification issue characterized by a high variance in the defect classes and probably overlapping decision regions. Therefore, we have to improve the signal processing algorithms, incorporate some type of expert knowledge, and obtain more ultrasonic signals from various types of defects or introduce modeling. It is important to note that we need compact data descriptions both to construct the classifier and for making the optimization (model tuning) feasible, which otherwise would be very time consuming.

[3]The basic idea is to tune the model to generate data which resembles the real measurement as much as possible.

References

[1] B. Eriksson and T. Stepinski. Ultrasonic charecterization of defects, part 1. literature review. Technical report, 1994. SKI Report 94:11.

[2] B. Eriksson and T. Stepinsk. Ultrasonic charecterization of defects, part 2. theoretical studies. Technical report, 1995. SKI Report 95:21.

[3] Bo Eriksson Tadeusz Stepinski and Bengt Vagnhammar. Ultrasonic charecterization of defects, part 3. experimantal varification. Technical report, 1996. SKI Report 96:75.

[4] Gilbert Strang and Truong Nguyen. *Wavelets and Filter Bank.* Wellesley - Cambridge Press, 1996.

[5] A. Boström. Ut defect: A model of ultrasonic ndt of cracks. In *7th European Conference on Non-Destructive Testing*, volume 3, pages 2414–2420, 1998.

[6] Keinosuke Fukanaga. *Introduction to Statistical Pattern Recognition.* Academic Press, second edition, 1990.

[7] P. Comon. Independent component analysis, a new concept? *Signal Processing*, 36(3):287–314, April 1994.

A Comparison of the 2.25 MHz and the 3.5 MHz Transducers

This section show a comparison of the 2.25 MHz and the 3.5 MHz transducers for some of the flaws found in the V-welded steel blocks. Below a number of figures are shown where each figure corresponds to one particular flaw. All of the figures (Figure 32–37) has 6 sub-figures, labeled (a),(b), ... ,(f), showing both B-scans, A-scans and the envelope of the A-scans. Each A-scan contains 1000 samples, which corresponds to an time interval of 25 μs, with the flaw response centered in the middle of this interval. Note also that the envelope is smoothed. The sub-figures (a)–(c) are for the 2.25 MHz transducer and the sub-figures (d)–(f) are for the 3.5 MHz transducer.

During data acquisition the aim has been to scan the defects at the same position for both the 2.25 MHz and the 3.5 MHz transducers. However, it is unavoidable to have some difference in probe position when changing transducer, which mostly shows in the response from the weld surface which shape is rather irregular and thus can give a large change in the US response signal for small probe position variations.

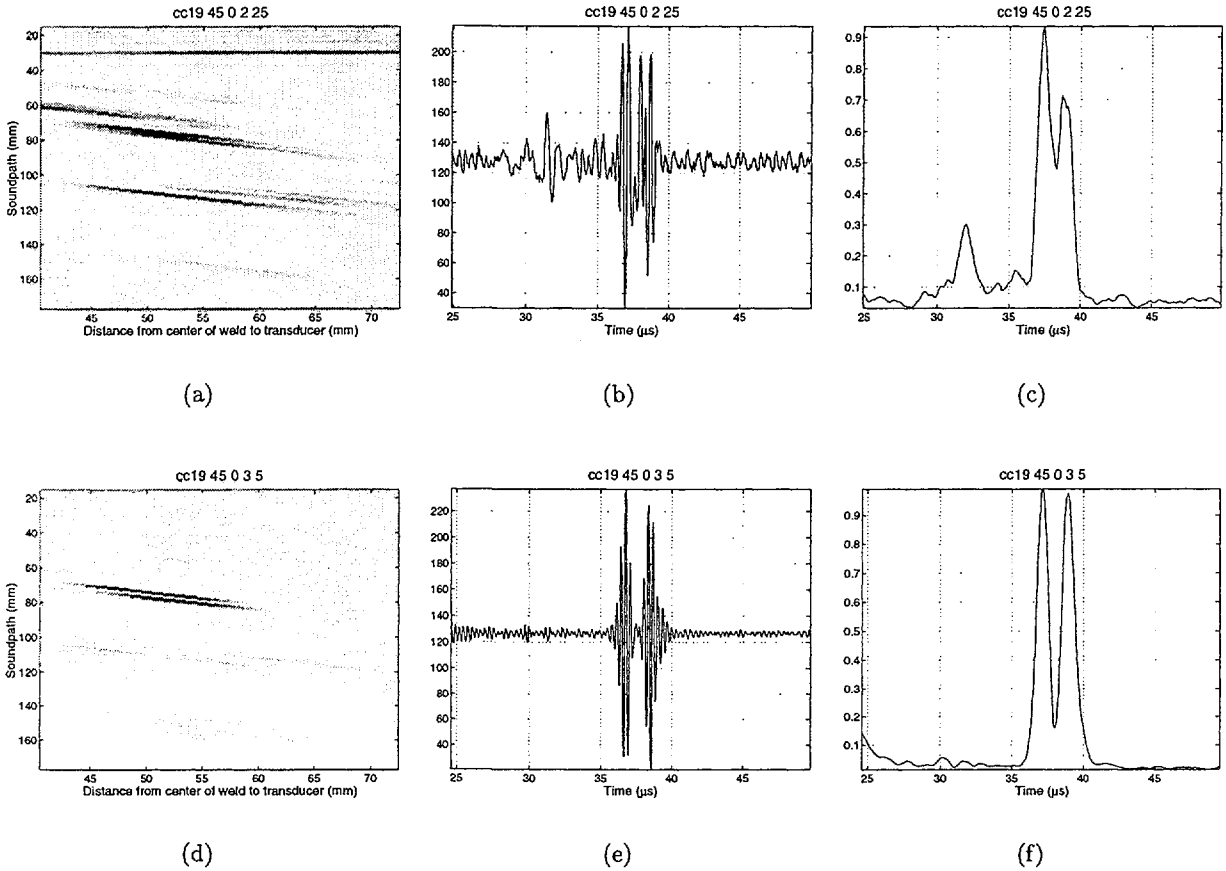

Figure 32: *Center crack #19 with the 45 degree wedge (A-scans at 52 mm from the weld).*

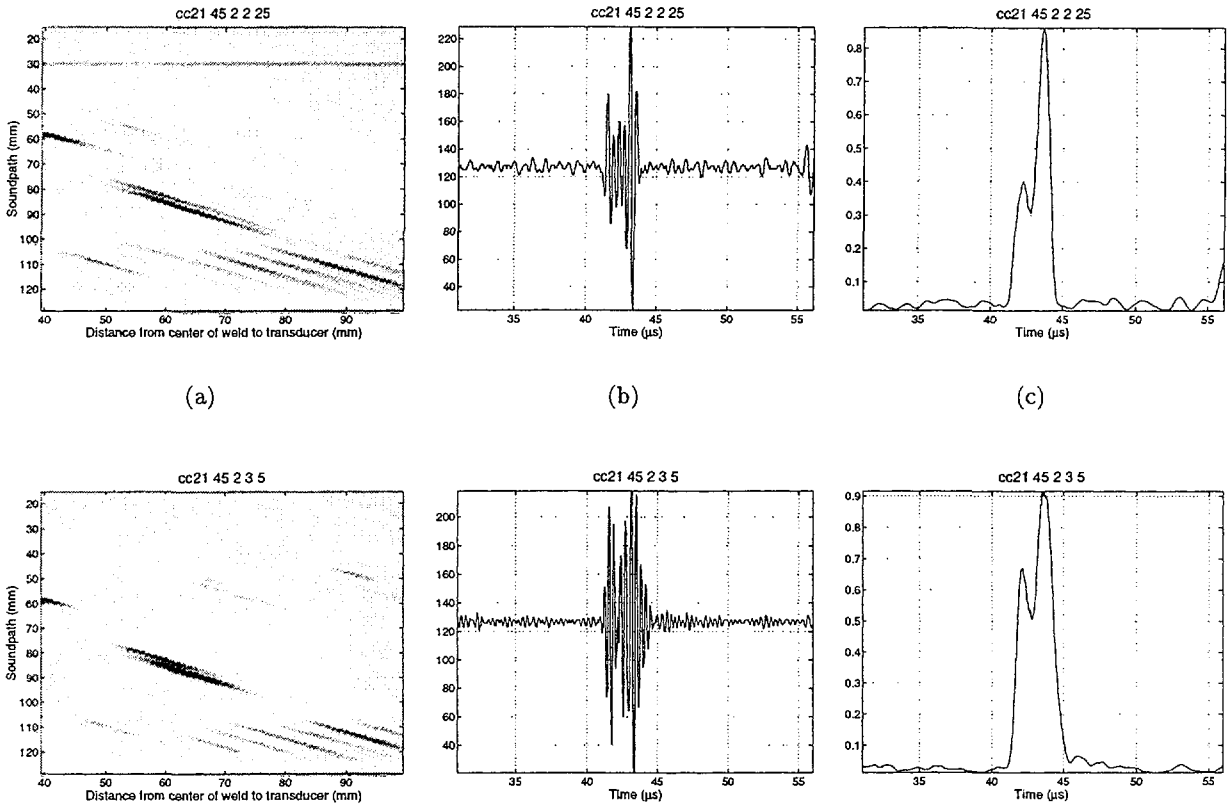

(a) (b) (c)

(d) (e) (f)

Figure 33: *Center crack #21 with the 45 degree wedge (A-scans at 62 mm from the weld).*

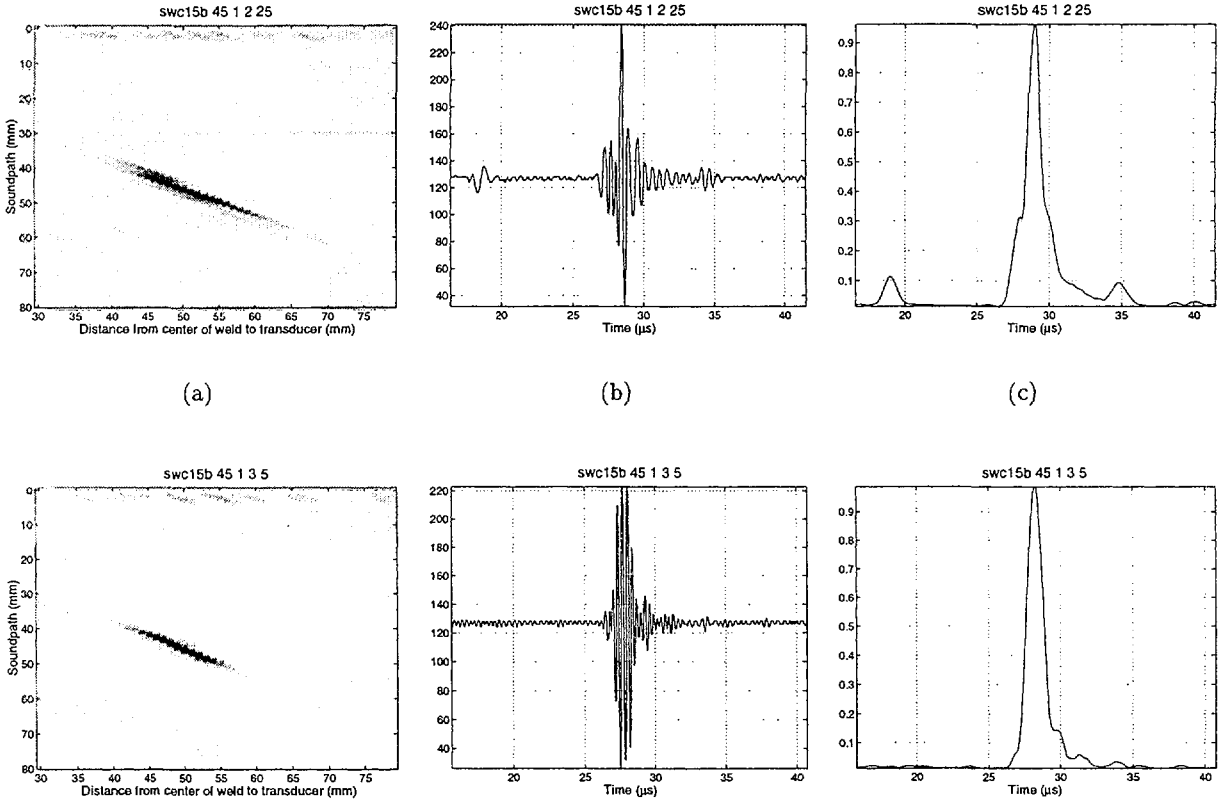

(a) (b) (c)

(d) (e) (f)

Figure 34: *Side wall crack #15 with the 45 degree wedge (A-scans at 50 mm from the weld).*

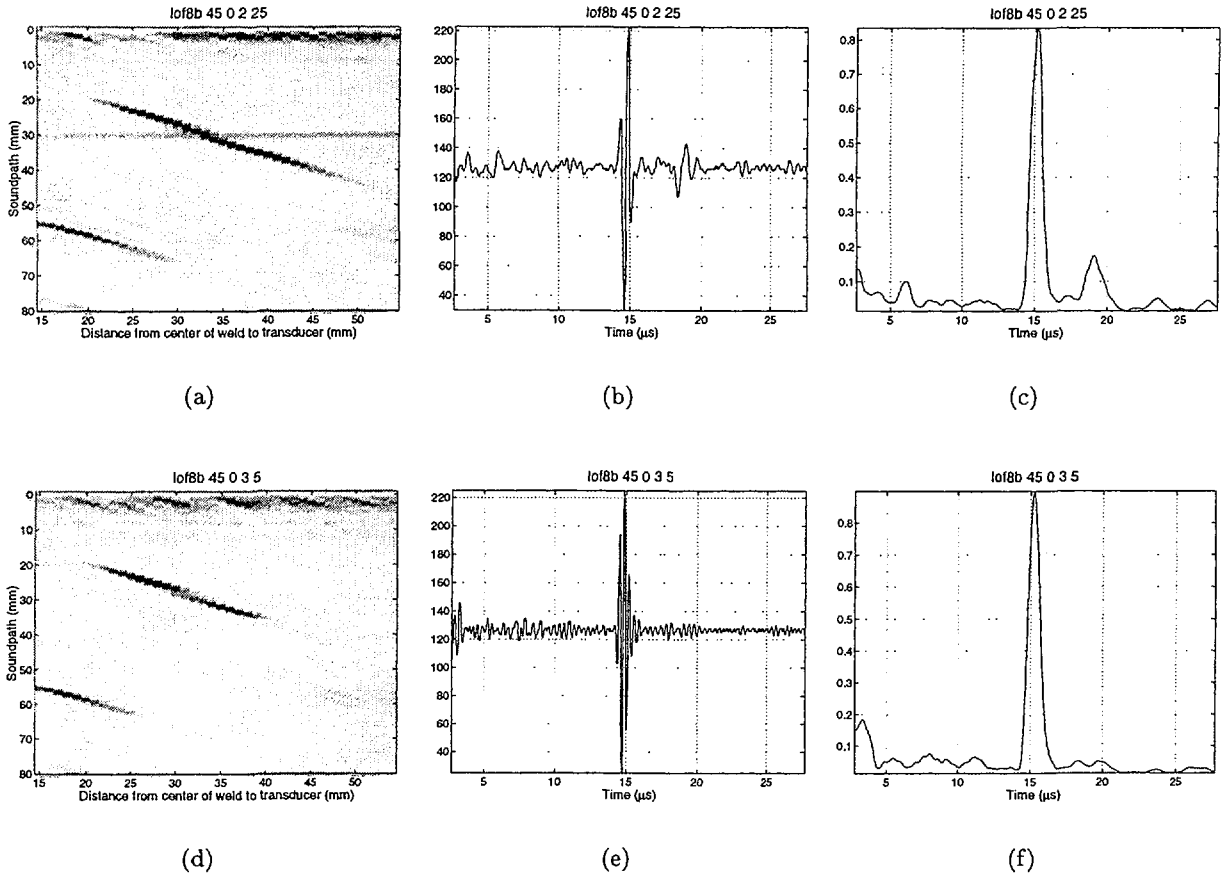

(a) (b) (c)

(d) (e) (f)

Figure 35: *Lack of fusion #8 with the 45 degree wedge (A-scans at 27 mm from the weld).*

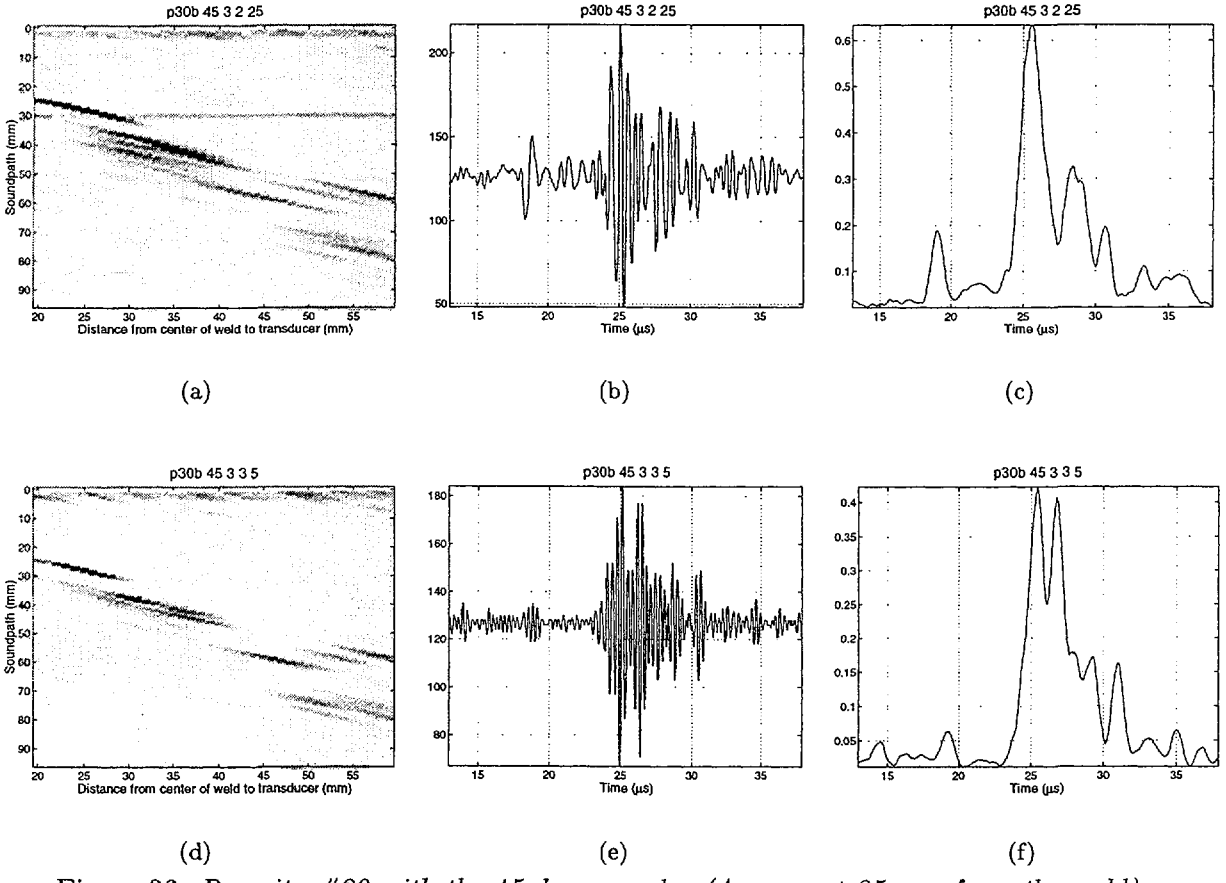

(a) (b) (c)

(d) (e) (f)

Figure 36: *Porosity #30 with the 45 degree wedge (A-scans at 35 mm from the weld).*

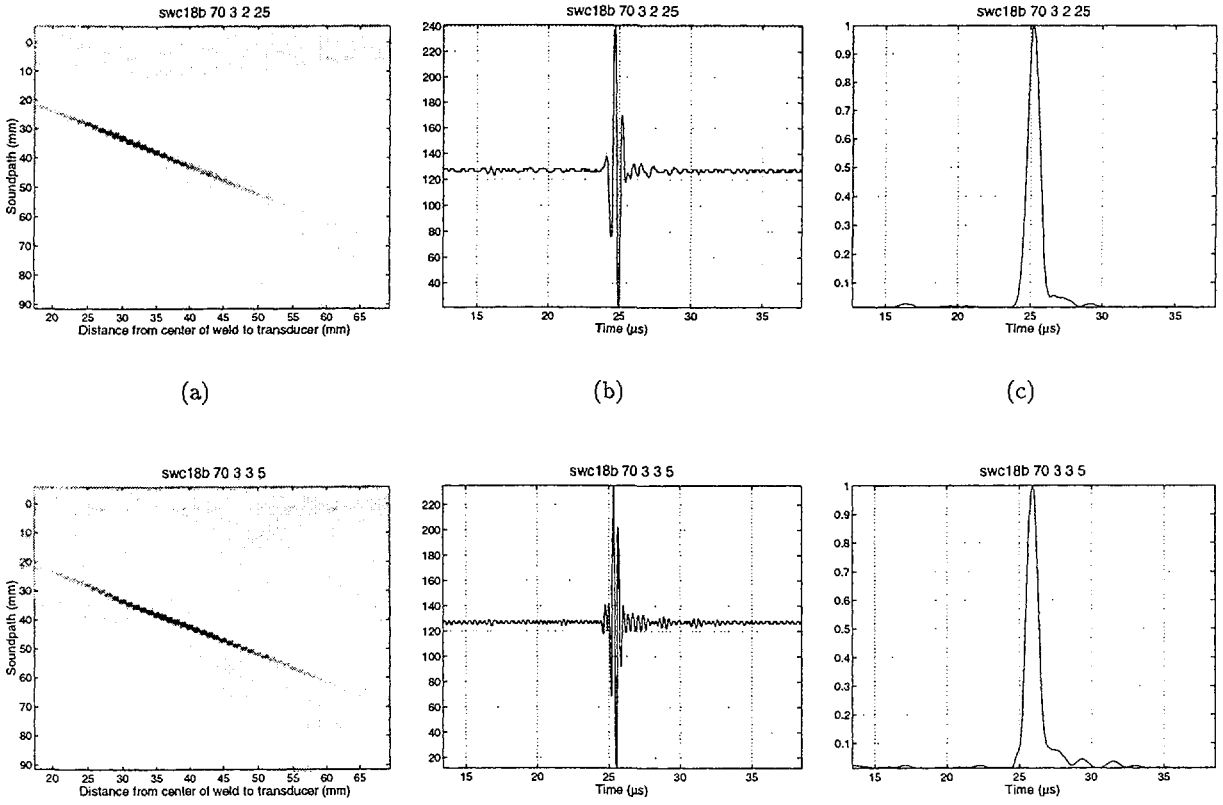

Figure 37: *Side wall crack #18 with the 70 degree wedge (A-scans at 33 mm from the weld).*

B Carbon Steel Block Drawings

B.1 PL4500

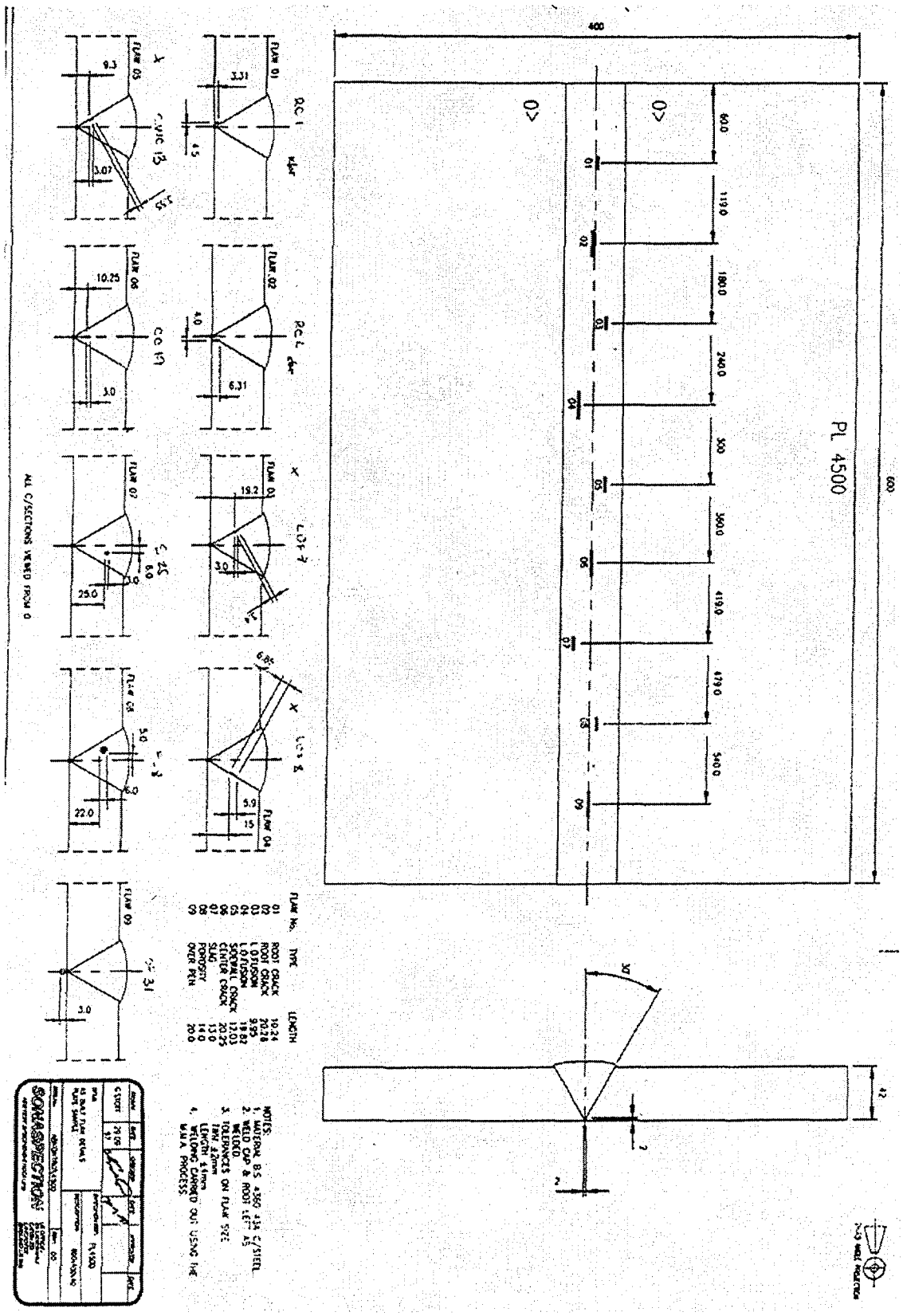

B.2 PL4501

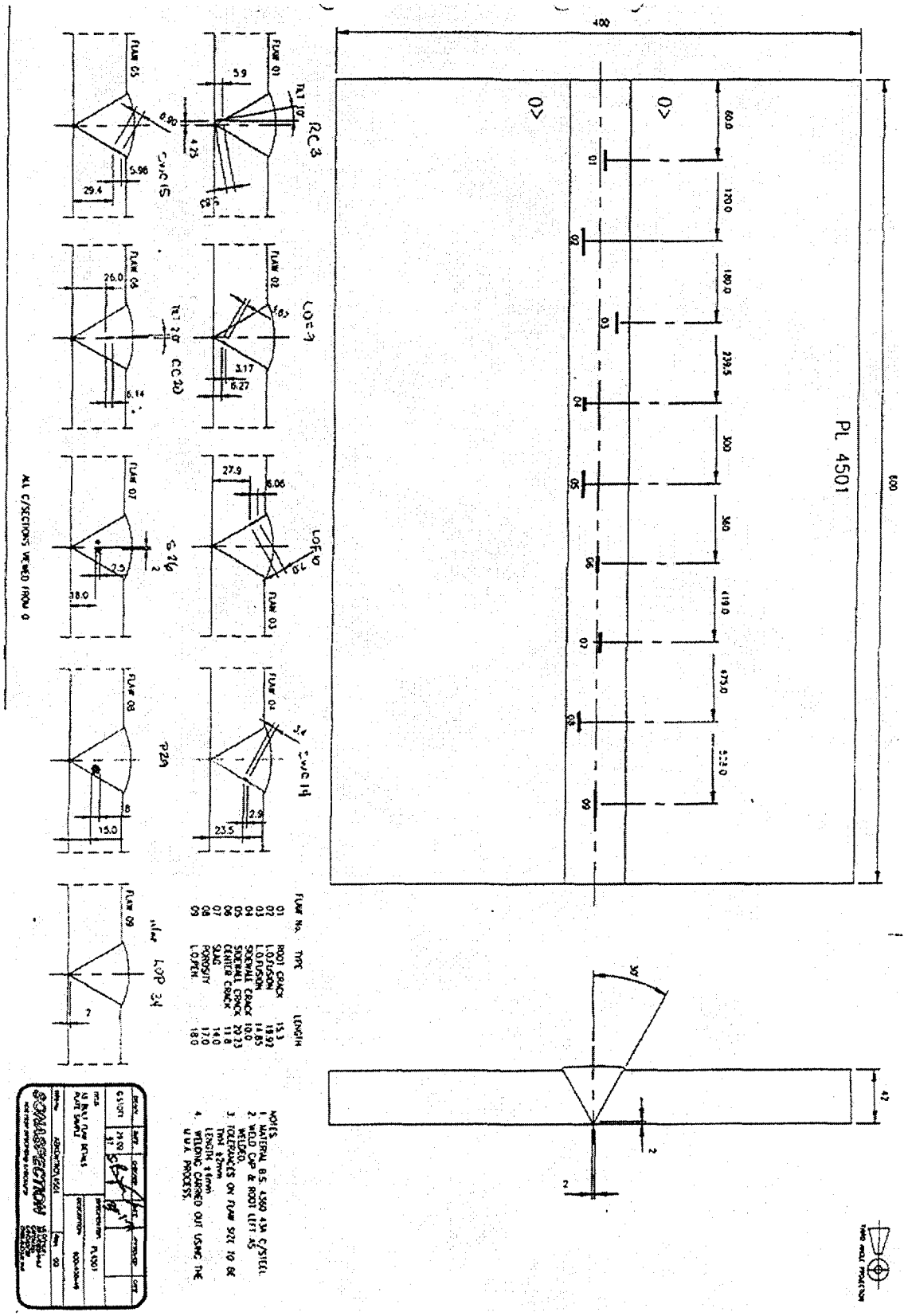
PL 4501
600
400
FLAW 01
FLAW 02
FLAW 03
FLAW 04
FLAW 05
FLAW 06
FLAW 07
FLAW 08
FLAW 09
ALL CROSSECTIONS VIEWED FROM O
NOTES
1. MATERIAL B.S. 4360 43A C/STEEL.
2. WELD CAP & ROOT LEFT AS WELDED.
3. TOLERANCES ON FLAW SIZE TO BE TWO ±2mm
LENGTH ±1mm
4. WELDING CARRIED OUT USING THE M.M.A. PROCESS.

B.3 PL4502

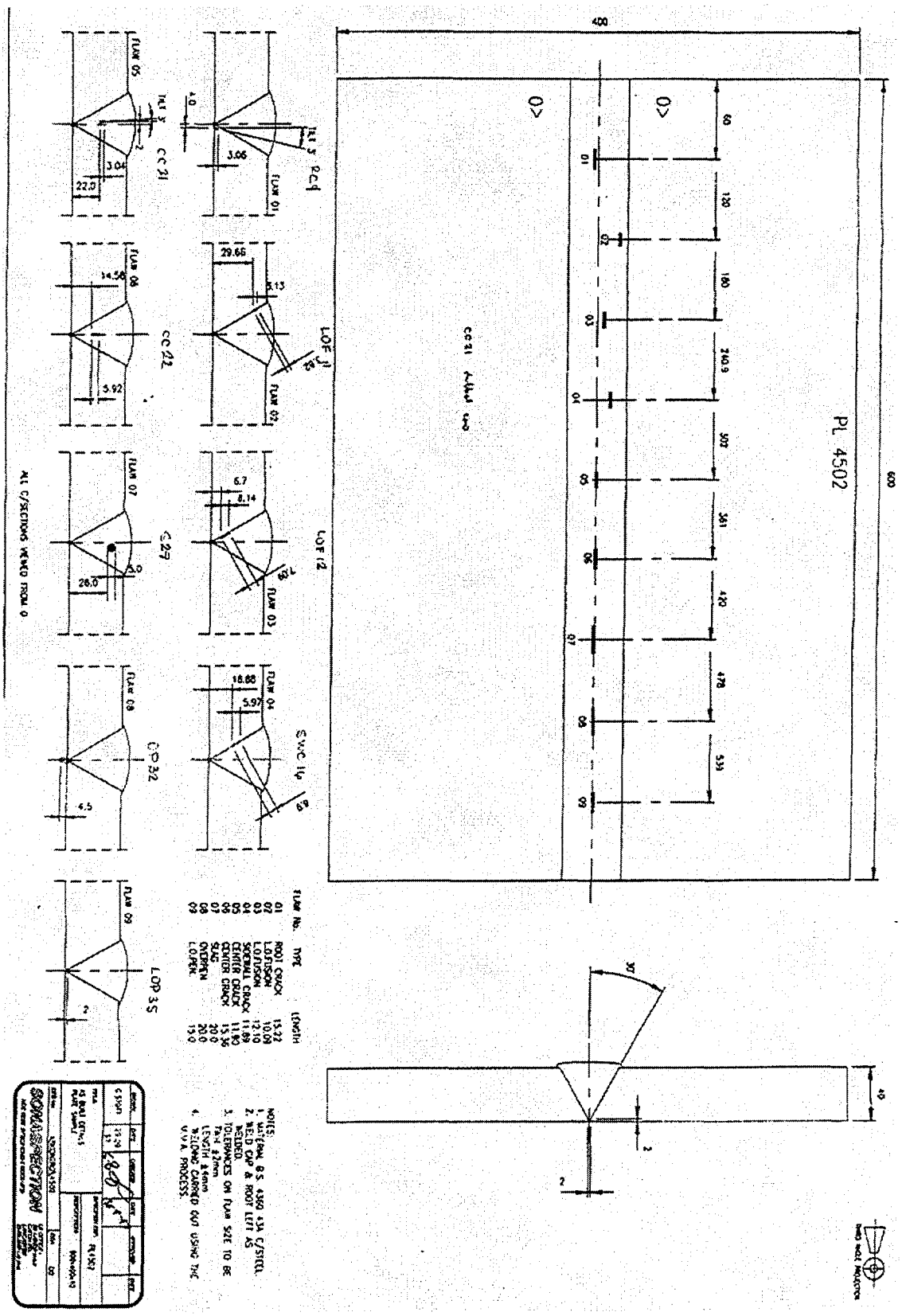
PL 4502
600
480
FLAW No. TYPE LENGTH
01 ROOT CRACK 15.22
02 LOF/SION 10.09
03 LOF/SION 12.10
04 SIDEWALL CRACK 11.89
05 CENTER CRACK 11.90
06 SLAG 15.36
07 OVERLAP 20.0
08 LOF/PEN 20.0
09 15.0
NOTES:
1. MATERIAL BS 4360 43A C/STEEL
2. WELD CAP & ROOT LEFT AS WELDED.
3. TOLERANCES ON FLAW SIZE TO BE T&I ±2mm LENGTH ±4mm
4. WELDING CARRIED OUT USING THE GMAW PROCESS.
CROSS SECTION
ALL C/SECTIONS VIEWED FROM 0

B.4 PL4503

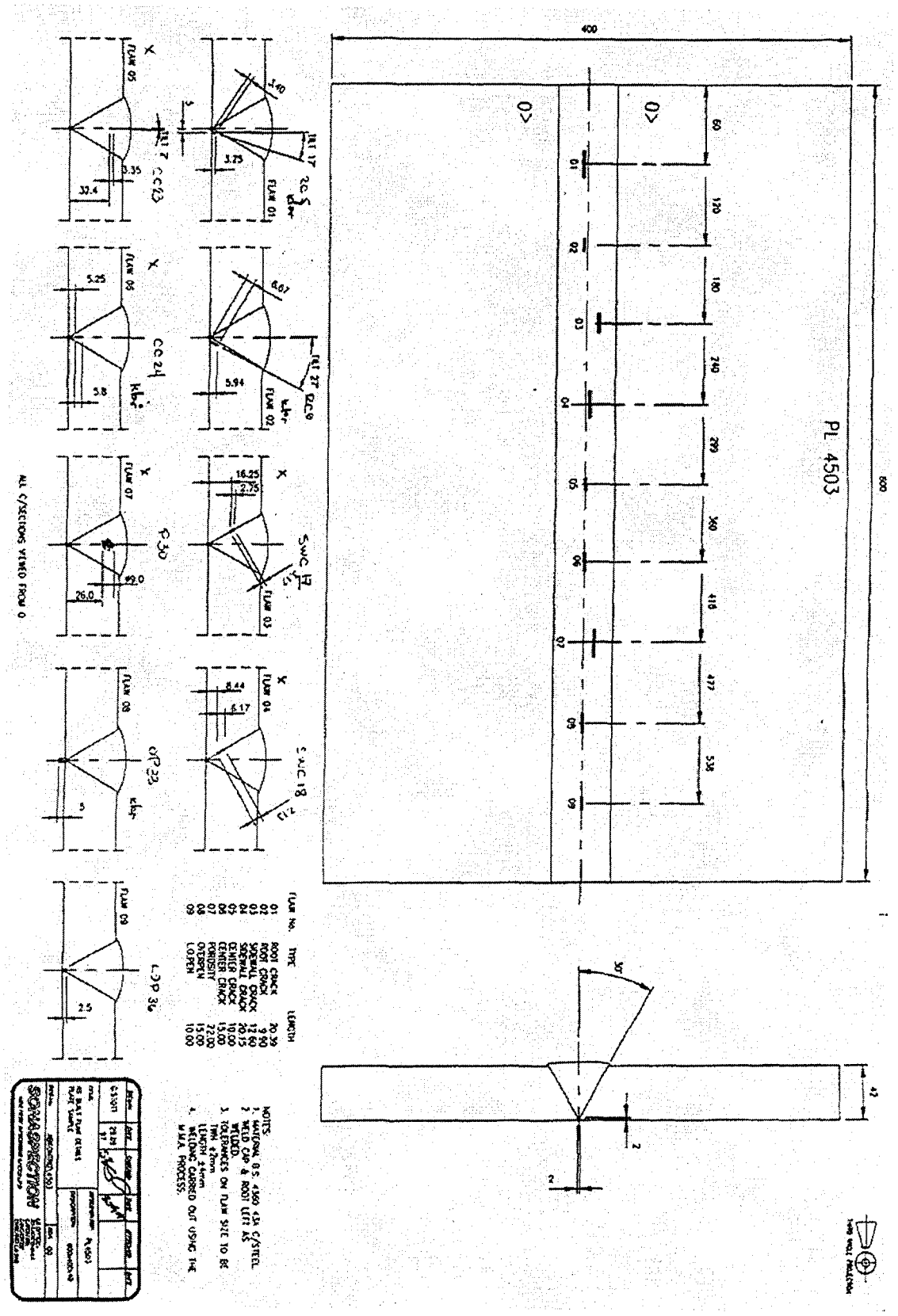
PL 4503
400
600
FLAW No. TYPE LENGTH
01 ROOT CRACK 70.39
02 ROOT CRACK 9.60
03 SIDEWALL CRACK 12.60
04 SIDEWALL CRACK 20.15
05 CENTER CRACK 10.00
06 CENTER CRACK 15.00
07 POROSITY 72.00
08 OVERLAY 15.00
09 LOPEN 10.00
NOTES:
1. MATERIAL BS 4360 43A C/STEEL
2. WELD CAP & ROOT LEFT AS WELDED.
3. TOLERANCES ON FLAW SIZE TO BE THK. ±2mm LENGTH ±4mm
4. WELDING CARRIED OUT USING THE M.M.A. PROCESS.
ALL C/SECTIONS VIEWED FROM O
THIRD ANGLE PROJECTION

www.ski.se

STATENS KÄRNKRAFTINSPEKTION
Swedish Nuclear Power Inspectorate

POST/POSTAL ADDRESS SE-106 58 Stockholm
BESÖK/OFFICE Klarabergsviadukten 90
TELEFON/TELEPHONE +46 (0)8 698 84 00
TELEFAX +46 (0)8 661 90 86
E-POST/E-MAIL ski@ski.se
WEBBPLATS/WEB SITE www.ski.se